Kinetics and Mechanism of the OH + C_6H_6 Reaction: A Detailed Analysis with First-Principles Calculations

I. V. Tokmakov and M. C. Lin*

Department of Chemistry, Emory University, 1515 Pierce Drive, Atlanta, Georgia 30322

Received: May 9, 2002; In Final Form: August 15, 2002

The capability of various high-level DFT and ab initio MO methods to predict molecular and energetic parameters has been critically tested for the OH radical reaction with benzene. G3 theory proved to be the most accurate in estimating reaction barriers and enthalpies. For the first time, the molecular structure, stabilization energy and nature of the bonding interactions of the [C_6H_6···OH] prereaction complex have been characterized. Accurate thermochemistry for major reaction channels was established by making combined use of experimental and theoretical parameters. A multistep kinetic model for the OH-addition channel was proposed, and the effects of *T*, *P*, and reaction time on the apparent rate constants were evaluated by weak collision master equation/RRKM analysis. Available experimental kinetic data for all relevant reactions are critically analyzed and correlated with modeled effective rate constants.

Introduction

The gas-phase chemistry of the OH radical is very important in high-*T* combustion as well as in low-*T* atmospheric processes. This radical acts as a scavenger by initiating tropospheric oxidation of such major anthropogenic pollutants as unsaturated hydrocarbons. Particularly important is the removal of aromatic hydrocarbons and PAH because of extensive environmental and health hazards presented by these pollutants. The development of macroscale models of complex atmospheric processes, such as those responsible for tropospheric ozone and smog formation over urban areas, puts a high demand on accurate kinetic data for elementary reactions describing the OH-radical-initiated atmospheric degradation of aromatic compounds.

The combustion of hydrocarbon fuels is another rapidly evolving area of macroscale kinetic modeling. Putting an emphasis on its competitive nature, Tsang characterized combustion as a "race between pyrolysis and oxidation".[1] Needless to say, OH radicals and small aromatics are among the key players in that competition. Whether a higher yield of oxidation products is desirable (as in combustion engines) or not (as in the fabrication of fullerenes and single-wall carbon nanotubes in fuel-rich flames), a detailed knowledge of oxidation mechanisms initiated by O_2, O, and OH radicals is of crucial importance for the determination of controlling parameters and the optimization of experimental conditions.

This study is concerned with a detailed mechanistic analysis of the OH radical reactions with benzene, the simplest aromatic compound. In the course of previous experimental *T*-dependence studies[2−18] and theoretical investigations,[19−23] the primary reaction modes of the OH radical attack on benzene have been identified as follows:

$$C_6H_6 + OH \rightarrow C_6H_5 + H_2O \quad (1)$$

$$C_6H_6 + OH \rightarrow C_6H_6OH \quad (2)$$

$$C_6H_6 + OH \rightarrow C_6H_5OH + H \quad (3)$$

where reaction 3 is a sequence of two elementary steps, namely, the OH addition to benzene (reaction 2) and the elimination of the H atom from the adduct (reaction 3′).

$$C_6H_6OH \rightarrow C_6H_5OH + H \quad (3')$$

Different pathways dominate under different experimental conditions. In the low-*T* regime, the OH-addition channel (eq 2) prevails, followed by the C_6H_6OH removal in secondary reactions. For instance, reactions with O_2 and NO result in several competing degradation pathways under tropospheric conditions.[24−26] Despite an abundance of experimental measurements near room *T* (RT),[6−12,17,27−37] an uncertainty still exists in the activation energy for reaction 2. As a result of extensive literature reviews,[2,3] small positive values of 0.6 ± 0.1 kcal/mol have been recommended for this parameter, whereas negative values from −0.7 to −2.8 kcal/mol appear in the Arrhenius expressions derived in the later studies.[11,17,18] The accuracy of experimental activation parameters is adversely affected by the reversibility of reaction 2. Above $T \approx 350$ K, the C_6H_6OH radical becomes unstable. In a fast equilibrium, the newly formed adducts preferably decompose back to the reactants:

$$C_6H_6OH \rightarrow C_6H_6 + OH \quad (-2)$$

In the high-*T* regime ($T > 450$ K), benzene decay is attributed almost entirely to the abstraction channel (eq 1). However, the discrepancy between different recommended rate constants for this channel reaches a factor of 5 at 400 K.[2,17] Several sources considered direct-displacement reaction 3 to be a viable competitor to H-abstraction at high *T*[38] and to OH addition at low *T*, where channel 3 may be responsible for a 25% yield of phenol at RT conditions.[27−29] However, the rates of H displacement by OH radicals obtained from QRRK analysis[20] and from kinetic studies of the reverse process[13] are so slow that they preclude its occurrence at RT.

Thus, despite an apparently large amount of available experimental data, not all mechanistic questions can be readily answered. The complexity of the reactions involved (particularly

* Corresponding author. E-mail: chemmcl@emory.edu.

10.1021/jp0211842 CCC: $22.00
Published on Web 10/25/2002

in the intermediate *T* range) leads to a nonexponential decay of reactants requiring extensive kinetic modeling to account for measured concentrations profiles. A lack of reliable kinetic parameters for various secondary reactions combined with narrow *T* ranges spanned by each experimental technique inevitably introduce additional uncertainty in the modeled rate constants and activation parameters.

The accuracy of theoretical results is less susceptible to *T* or other conditions. Theoretical errors are more predictable and often can be accounted for in a systematic manner. Hence, theoretical studies could provide a valuable complement to the experimental data. The consistency of both theory and experiment is ultimately required for the interpretation of the mechanism and for reliable kinetic data. Prior theoretical investigations of the OH + C_6H_6 reactions by semiempirical MO methods (MINDO/3,[19] PM3,[20] and AM1[21]) have been very limited in their success. Activation barriers are strongly overestimated by these methods. The corrections needed are so large (tens of kcal/mol) that they effectively diminish the predictive power of theoretical results. Consequently, the rate-constant calculations were rarely performed. The only study that provided calculated rate constants was the QRRK analysis of Lay, Bozzelli, and Seinfeld.[20] However, they used empirical rather than theoretically predicted reaction barriers and fitted degenerate vibrational frequencies to evaluate *T* and *P* effects on the apparent rate constants for channels 2 and 3 and some other related reactions. Berho, Rayez, and Lesclaux[22] employed the B3LYP/6-31G(d) density functional for geometry optimization and BAC-MP4 single-point calculations to obtain energetic parameters, but the scope of their study was limited to the X−C_6H_6 bond-dissociation energies for a series of substituted cyclohexadienyl radicals. The more recent work of Barckholtz, Barckholtz, and Hadad[23] focused on the elucidation of the initial reaction mechanism of the H, O, and OH radicals with a series of aromatic compounds. Their rate constants for the OH + C_6H_6 reactions calculated on the basis of B3LYP energetic and molecular parameters significantly depart from the experimental counterparts both in absolute and relative values. For instance, the predicted preference of H abstraction (1) at RT over OH addition (2) is in sheer contradiction with experiment. No attempt was made on correcting theoretical deficiencies to obtain more reliable rate constants. Given the importance of the OH + C_6H_6 system, we feel that it deserves more attention from a theoretical standpoint. In this work, we will present detailed potential energy profiles for all reaction modes calculated by various DFT and high-level ab initio MO methods. Then the rate constants for all elementary steps will be calculated by statistical theories and analyzed with respect to experimental data.

Computational Methods

Geometry optimizations of the reactants and products were performed with second-order Moller−Plesset perturbation theory (MP2) as well as with B3LYP[39] (Becke's three-parameter gradient-corrected exchange functional with the gradient-corrected correlation functional of Lee, Yang, and Parr), MPW1K[40] (modified Perdew−Wang one-parameter model optimized against 20 forward and reverse reaction barriers), and KMLYP[41] (two-parameter model combining a mix of HF and Slater exchange functionals with a mix of Vosko−Wilk−Nusair (VWN) and Lee−Yang−Parr (LYP) correlation functionals) density functional theories with several basis sets. Intrinsic reaction coordinate (IRC) calculations[42] allowed us to obtain accurate reaction profiles and make unambiguous connections between the stationary points located on the reaction paths. Tight convergence criteria were reinforced in both geometry and electronic wave function optimizations. Unscaled vibrational frequencies were employed for the calculation of zero-point energy (ZPE) corrections, the characterization of stationary points, and rate-constant calculations. All energies herein include a ZPE correction unless specifically noted.

For a more accurate evaluation of the energetic parameters, higher-level single-point calculations were carried out on the lower-level optimized structures. Upon a comparison of the calculated molecular parameters with available experimental data for the reactants and products (vide infra), the B3LYP density functional with the 6-311++G(d,p)[43] basis set was chosen as the lower-level geometry optimization method. At the higher level, we performed a series of QCISD(T), CCSD(T), MP4, and MP2 calculations with various basis sets as a part of G2M[44] and G3[45] model chemistries. A quadratically convergent SCF procedure[46] provided all post-SCF methods with an initial Hartree−Fock wave function. For all of them, a frozen core (FC) approximation was in effect, except for the MP2/G3Large calculation, which included all electrons (FU) in a correlation calculation.

The G2M method[44] was originally based on the B3LYP/6-311G(d,p) geometries and frequencies, and several schemes were proposed to approximate the CCSD(T)/6-311+G(3df,2p) energetic parameters with a "higher-level correction" (HLC) that depends on the number of paired and unpaired electrons. The G2M(CC,MP2) scheme is chosen in this study as the most accurate and is still affordable for the present system with open-shell seven-heavy atoms. More details on the presently employed G2M(CC,MP2)//B3LYP/6-311++G(d,p) version of the G2M method are given in our previous work.[47]

Gaussian-3 theory[45] was found to be less computationally demanding and more accurate than its predecessors, including the G2[48] and G2M[44] methods. In its limit, G3 theory approximates the QCISD(T,FU)/G3Large level and includes an additional (empirical) HLC and a spin−orbit correction for atoms. The B3LYP density functional with 6-31G(d) and 6-31G(2df,p) basis sets was originally employed for geometry optimization in the G3//B3LYP[49] and G3X[50] versions of G3. We have analyzed the performance of B3LYP/6-311++G(d,p) and B3LYP/6-31G(2df,p) density functionals for a limited set of H-, C-, and O-containing compounds relevant to the present study. The optimized geometrical parameters were very similar and very close to the available experimental values. The vibrational frequencies were also in good agreement; however, the B3LYP/6-311++G(d,p) values generally had smaller deviations from the experiment. The calculations with the 6-311++G(d,p) basis set were also faster than analogous calculations with the 6-31G(2df,p) basis set. Therefore, we favored B3LYP/6-311++G(d,p) over the originally proposed B3LYP/6-31G(2df,p) method for geometry optimizations in G3 calculations. Furthermore, the consistent use of the same level of theory for geometry optimization also permitted us to make a more accurate comparison of the G2M and G3 theoretical parameters obtained in this study with our previous G2M results for related C_6H_6 + CH_3 and C_6H_6 + H reactions.[47,51]

For brevity, the following short notations for basis sets will be used in this work: (I) for 6-31++G(d,p), (II) for 6-311++G(d,p), and (III) for 6-31G(2df,p). Results calculated at the G2M(CC,MP2)//B3LYP/6-311++G(d,p) and G3//B3LYP/6-311++G(d,p) levels of theory will be denoted simply as G2M and G3. We should note that all reactions considered in this study are isogyric (the number of electron pairs is conserved), resulting

in the cancellation of HLCs for all relative energies. Hence, all predicted barriers and enthalpies of reaction are effectively independent of the empirical coefficients in the HLCs. However, those coefficients have to be reoptimized for the present variations of G2M and G3 theories before they can be used for atomization energy calculations and any nonisogyric reactions in general. For all DFT and ab initio MO calculations, the Gaussian 98 program package[52] was used.

The rate-constant calculations were carried out with the recently updated version 1.19 (Feb. 20, 2002) of the ChemRate program[53] from NIST. This program provides the computational means for accounting for non-steady-state effects in complex kinetic schemes including chemical activation, isomerization, collisional energy transfer, and unimolecular decomposition processes. The usual energetic and molecular parameters (reaction barriers, moments of inertia, and vibrational frequencies) are required as input for the sum and density-of-states computations, followed by the microscopic rate-constant $k(E)$ calculations by RRKM theory.[54−56] In the present study, the energy increment was fixed at 10 cm^{-1} in all sum and density-of-states calculations that were performed using the modified Beyer−Swinehart algorithm.[57] The standard form of the "exponential-down" model[55,58] was used for collisional energy transfer. This model requires the $\langle \Delta E \rangle_{down}$ parameter (average energy loss per collision of the active component with a bath gas molecule) on the input. We used fitted (where available) or assumed values of this parameter since no other theoretical or experimental estimates could be found. The frequency of collisions with the bath gas was estimated from the Lennard-Jones parameters adopted from Reid et al.[59] Finally, the apparent *P*-, *T*- and *t*-dependent rate constants have been obtained after solving the master equation,[55] which describes the evolution of all active components. The present approach to solving the master equation consists of two steps: (1) the master equation is expressed in matrix form and then (2) the eigenvalues/eigenvectors problem is solved by a method based on Householder's tridiagonalization algorithm.[60] The default energy bin size of $\delta E = 100$ cm^{-1} was used in the master equation computations, and the matrix size was 526×526. More details about the implementation of the time-dependent master equation/RRKM analysis in ChemRate are available from a series of publications of Tsang and coauthors.[61]

Results and Discussion

An adequate description of the energetics and electronic and molecular structures of aromatic and highly delocalized radicals involved in the present study requires a sophisticated treatment of electron correlation in combination with large basis sets. Unfortunately, current limitations of available computer resources prohibit extensive searches on the potential energy surfaces (PES) obtained with highly correlated methods and basis sets of a size sufficient to approach the limit of infinite expansion. During the past decade, however, a novel approach of model chemistries was successfully introduced and has been rapidly evolving ever since. This approach takes advantage of the separability of certain theoretical deficiencies and relatively small displacements of stationary points on the PES calculated with different but sufficiently accurate methods. On the basis of the last assumption, the higher-level energy of a given chemical species can be approximated from a single-point high-level calculation at the geometry optimized on the lower-level PES. The choice of the lower-level method is, therefore, important for the good performance of the whole scheme.

Two high-level theories will be used in this work, namely, G2M[44] and G3.[45] Previously, several implementations have been suggested using B3LYP and MP2 theories as lower-level optimization methods. In the following section, the performances of these theories at the 6-31++G(d,p) level are compared to each other and to the MPW1K[40] and KMLYP[41] density functionals, which have been suggested recently for the prediction of accurate reaction barriers and enthalpies within the framework of DFT. The effect of basis-set expansion to 6-311++G(d,p) and 6-31G(2df,p) is tested for B3LYP-optimized geometries of some molecules relevant to this study.

A. Analysis of Selected Geometry Optimization Methods. The geometric parameters of the reactants and products of the C_6H_6 + OH reactions optimized by selected methods are listed in Table 1. Also in Table 1, the list of geometrical parameters for each molecule is followed by the average of the absolute relative deviations of calculated vibrational frequencies from the experiment. The experimental data for OH and H_2O is taken from a NIST compilation.[62] Electron diffraction intensities and microwave spectroscopy of benzene[63] and phenol[64] were used to determine their r_g- and r_s-type molecular structures. Averages of r_g and r_s geometric parameters have been adopted in this study for comparison with theory. A complete set of observed vibrational frequencies for benzene[65] and phenol[66] is also available for testing the quality of theoretical predictions. The vibrational spectrum of the phenyl radical in an Ar matrix has been updated recently,[67] and now all but the lowest A_2 vibrational frequency have been assigned from the experimental infrared[68] and Raman[69] spectra. We questioned[51] five earlier assignments[70] of the C_6H_5 vibrational frequencies. Four of them have been corrected, and those were the four largest corrections introduced in the updated version.

The molecular structures of OH, H_2O, C_6H_6, and C_6H_5OH are accurately predicted by MP2/(I) and B3LYP/(I) theories. The agreement with experimental bond lengths is within 0.01 Å for O−H and even better for C−H, C−C, and C−O bonds. The majority of calculated bond lengths and valence angles are within the uncertainty limits of the experimental values (typically, ±0.005 Å for distances and ±0.5° for angles). We note that the H-atom substitution for OH causes a relatively small distortion of the benzene ring. Therefore, theoretical C−C and C−H bond lengths and C−C−C valence angles β and γ (at the ortho and meta carbons) have been averaged in order to be compared to the experimental counterparts, which were derived with assumptions about the local C_{2v} symmetry of the C_6H_5 group in phenol.[64]

Considerable differences between B3LYP/(I) and MP2/(I) molecular parameters arise for phenyl. The molecular structure of C_6H_5 optimized at the B3LYP/(I) level features C−C bonds at the radical site (r(C1−C2)) that are shortened by ca. 0.02 Å and small changes in the length of the other four C−C bonds compared to those of benzene. At the MP2/(I) level, however, all six C−C bonds are tightened relative to the C−C bonds in benzene. They become 0.04 Å shorter at the radical site and shorten half as much at the remaining positions. No experimental structure of the free phenyl radical is available for comparison. However, the quality of theoretical molecular structures can be judged by other molecular parameters such as vibrational frequencies (see Tables 1 and 2). Clearly, the B3LYP/(I) method provides a good approximation of the experimental vibrational spectrum of C_6H_5 with a mean absolute deviation of 2.3%, whereas the MP2/(I) theory performs very poorly with a mean absolute deviation of 9.5% and an absolute deviation of more than 20% for several individual frequencies. Similar problems with MP2 theory at the 6-31G(d,p) level have been encountered previously.[68] Apparently, a basis-set expansion to include

TABLE 1: Performance of Selected Geometry Optimization Methods

parameter[a]	B3LYP/(I)	MPW1K/(I)	KMLYP/(I)	MP2/(I)	B3LYP/(II)	B3LYP/(III)	expt[b]
			OH ($C_{\infty v}$, $^2\Gamma_i$)				
r(O−H)	0.980	0.967	0.963	0.974	0.976	0.976	0.971
$<\lvert\nu_{th} - \nu_{exp}\rvert/\nu_{exp}>$	1.4%	6.4%	7.9%	4.7%	1.6%	1.2%	
			H_2O (C_{2v}, $^1A_1$)				
r(O−H)	0.965	0.953	0.950	0.963	0.962	0.962	0.957
∠(H−O−H)	105.7	106.2	106.9	105.4	105.1	103.7	104.5
$<\lvert\nu_{th} - \nu_{exp}\rvert/\nu_{exp}>$	3.0%	7.2%	8.2%	4.7%	3.1%	4.3%	
			C_6H_6 (D_{6h}, $^1A_{1g}$)				
r(C−C)	1.398	1.387	1.380	1.399	1.395	1.394	1.396
r(C−H)	1.086	1.080	1.077	1.083	1.084	1.085	1.085
$<\lvert\nu_{th} - \nu_{exp}\rvert/\nu_{exp}>$	2.5%	5.7%	7.4%	3.8%	2.2%	2.4%	
			C_6H_5OH (C_s, $^1A'$)				
$<r$(C−C)$>$	1.399	1.387	1.379	1.398	1.394	1.394	1.396
$<r$(C−H)$>$	1.086	1.080	1.077	1.083	1.084	1.085	1.085
r(C1−O)	1.372	1.353	1.342	1.379	1.370	1.364	1.378
r(O−H)	0.966	0.954	0.951	0.967	0.963	0.963	0.958
∠C2−C1−C6 (α)	120.2	120.1	120.1	120.4	120.2	120.0	121.3
∠C1−C2−C3 (β)	119.6	119.7	119.7	119.5	119.6	119.7	119.1
∠C2−C3−C4 (γ)	120.6	120.7	120.6	120.5	120.6	120.6	120.6
∠C3−C4−C5 (δ)	119.3	119.2	119.2	119.4	119.3	119.3	119.4
∠C2−C1−O	122.5	122.5	122.4	122.7	122.5	122.6	122.1[c]
∠C1−O−H	110.0	110.2	110.9	109.1	109.7	109.0	108.8[c]
$<\lvert\nu_{th} - \nu_{exp}\rvert/\nu_{exp}>$	2.4%	5.8%	7.5%	4.7%	2.0%	3.1%	
			C_6H_5 (C_{2v}, $^2A_1$)				
r(C1−C2)	1.379	1.370	1.363	1.357	1.374	1.374	
r(C2−C3)	1.406	1.394	1.386	1.376	1.403	1.402	
r(C3−C4)	1.399	1.389	1.381	1.374	1.396	1.394	
$<r$(C−H)$>$	1.086	1.080	1.077	1.082	1.084	1.085	
∠C2−C1−C6 (α)	125.9	125.8	125.9	125.8	126.0	125.9	
∠C1−C2−C3 (β)	116.5	116.5	116.5	116.4	116.5	116.5	
∠C2−C3−C4 (γ)	120.2	120.2	120.2	120.6	120.2	120.2	
∠C3−C4−C5 (δ)	120.6	120.6	120.6	120.3	120.7	120.7	
$<\lvert\nu_{th} - \nu_{exp}\rvert/\nu_{exp}>$	2.3%	5.8%	7.5%	9.5%	2.2%	2.4%	

[a] Bond lengths are given in angstroms, and angles are given in degrees. [b] Experimental molecular structure data was taken from ref 62 for OH and H_2O; molecular parameters were averaged between the values determined by electron diffraction and microwave spectroscopy for benzene[63] and phenol.[64] [c] From ref 64b.

diffusion functions does not cure the theoretical deficiencies of this method in the calculation of the molecular structure of the phenyl radical.

For the other molecules listed in Table 1, vibrational frequencies predicted at the MP2/(I) level are more accurate, with mean absolute deviations of 4−5% from the experimental values. However, this is still worse than the 2−3% deviations exhibited by the B3LYP/(I) frequencies.

The molecular parameters obtained at the MPW1K/(I) and KMLYP/(I) levels of theory systematically underestimate bond lengths and overestimate vibrational frequencies. Molecular structures optimized with the KMLYP functional are particularly tight. In contrast to the performance of MP2 theory, the performance of these density functionals does not deteriorate for phenyl radicals, which makes them more acceptable for systematic use as a geometry optimization method. However, it is the B3LYP density functional that consistently yields accurate molecular structures and the closest matches to the experimental vibrational spectra of the species examined in this section.

The quality of the B3LYP molecular parameters further improves with basis-set expansion. The results obtained with basis set (I), (II), and (III) are compared in Table 1. Our choice of (II) is dictated by our previous experience of using the B3LYP/(II) level of theory for the geometry optimization of related aromatic hydrocarbons,[47,51] whereas the B3LYP/(III) was recommended as a reliable geometry optimization method for the G3X family of methods.[50] The basis-set size increases from (I) to (III) so that for a C_6H_7O molecular system these sets contain 175, 203, and 231 basis functions, respectively. Evidently, the molecular geometries are not strongly influenced by the basis-set expansion beyond (I), and the structural parameters obtained by the B3LYP theory with basis sets (II) and (III) are particularly similar. The best agreement of vibrational frequencies with experiment is obtained not with the largest basis set (III) but with (II). This probably reflects the importance of adding to the basis set diffuse rather than extra polarization functions for a more accurate calculation of the vibrational spectra of the present π-electronic systems.

The last factor that should be taken into account when choosing the method of geometry optimization is speed. The computational time increases for the methods discussed in this section in the following manner: B3LYP/(I) ≤ KMLYP/(I) ≈ MPW1K/(I) < B3LYP/(II) < B3LYP/(III) ≪ MP2/(I). Therefore, the B3LYP/(I) level of theory would be a good compromise between speed and accuracy for the present system and for larger molecular systems. Nevertheless, our favorite method is B3LYP/(II) on the basis of its performance for the molecules and radicals examined in this section.

Therefore, all higher-level calculations discussed in the following sections have been carried out on the B3LYP/(II)-optimized geometries. Vibrational frequencies calculated at the same level of theory have been used without any adjustment. We advocate the use of unscaled B3LYP/(II) vibrational frequencies mainly because the adjustment of low and high frequencies by a uniform scaling factor is not well justified. It has been shown previously[71] that different scaling factors are more suitable for different purposes (to fit experimental

TABLE 2: Moments of Inertia[a] (I_A, I_B, I_C), Symmetry Numbers (n), and Vibrational Frequencies of the Species Involved in the OH + C_6H_6 Reaction

		frequencies (ν/cm^{-1})		
molecule	I_A, I_B, I_C/10^{-40} g cm^2	symmetry	calculated[a]	experimental[b]
OH	1.50	Σ	3709	3652
H_2O	1.02, 1.95,	A_1	1603, 3817	1595, 3657
$n = 2$	2.97	B_2	3922	3756
C_6H_6	147.1,	A_{1g}	1011, 3192	993, 3074
$n = 12$	147.1,	A_{2g}	1381	1350
	294.3	A_{2u}	686	674
		B_{1u}	1022, 3155	1010, 3057
		B_{2g}	719, 1011	707, 990
		B_{2u}	1175, 1335	1150, 1309
		E_{1g}	862	849
		E_{1u}	1059, 1510, 3181	1038, 1484, 3057
		E_{2g}	622, 1197, 1633, 3166	608, 1178, 1610, 3050
		E_{2u}	410, 980	398, 967
C_6H_5	133.3,	A_1	619, 987, 1014, 1049,	605, 973, 998, 1028,
$n = 2$	149.4,		1175, 1468, 1570,	1151, 1439, 1497,
	282.8		3156, 3174, 3188	3037, 3072, 3086
		A_2	399, 812, 962	(?)[c], 816, 945
		B_1	424, 665, 719, 892, 984	415, 655, 703, 873, 990
		B_2	600, 1071, 1176,	588, 1060, 1159,
			1301,1324, 1461,	1281, 1310, 1432,
			1627, 3162, 3177	1593, 3060, 3070
C_6H_5OH	148.1,		228, 314, 405, 417,	225, 309, 403, 409,
	320.6,		509, 536, 633, 674,	503, 526, 619, 686,
	468.6		751, 820, 827, 879,	751, 817, 823, 881,
			952, 972,1013, 1043,	958, 973, 999, 1025,
			1093, 1177, 1191,	1070, 1150,1168,
			1192, 1275,1349,	1176, 1261, 1277,
			1368, 1499, 1527,	1343, 1472, 1501,
			1635, 1646, 3149,	1603, 1610, 3027,
			3167,3176, 3190,	3049, 3063, 3070,
			3197, 3836	3087, 3656

[a] Calculated at the B3LYP/(II) level. [b] Experimental frequencies are from refs 62 (OH and H_2O), 65 (C_6H_6), 66 (C_6H_5OH), and 67 (C_6H_5). [c] No experimental value is reported.

fundamentals, harmonic frequencies, ZPE, or vibrational partition functions). The proposed scaling factors for vibrational frequencies obtained from B3LYP calculations with sufficiently large basis sets modify them by less than 2%; the adjustment is even smaller when using a scaling factor optimized for low frequencies,[71] thus making negligible the effect of frequency scaling on relevant thermodynamic functions. Overall, small deviations from the available experimental values validate the use of unscaled B3LYP/(II) vibrational frequencies in this study.

B. Potential Energy Profiles and Molecular Structure of the Intermediates and Transition States. H-Abstraction Channel. Illustrated in Figure 1 are the potential energy profiles for two reactive modes of the OH radical attack on benzene. The first channel is the H-atom abstraction from benzene; it proceeds in a single step via the transition state TS1 and yields water and a phenyl radical. The molecular structure of TS1 (see Figure 2) reflects its transitional nature: the breaking C−H bond is elongated by 0.16 Å, and the forming O−H bond is 0.30 Å longer than its equilibrium value in the products. The second O−H bond is not directly involved in the reaction, but it becomes stronger and its length decreases by 0.014 Å as another H atom transfers to the O atom. The transient length of this bond is slightly closer to that of the OH reactant. The bonds and valence angles in the C_6H_5 fragment of TS1 are intermediate between the corresponding values in benzene and the phenyl radical. The overall structure of TS1 is slightly closer to that of the reactants, which is in accordance with the small exothermicity of reaction 1.

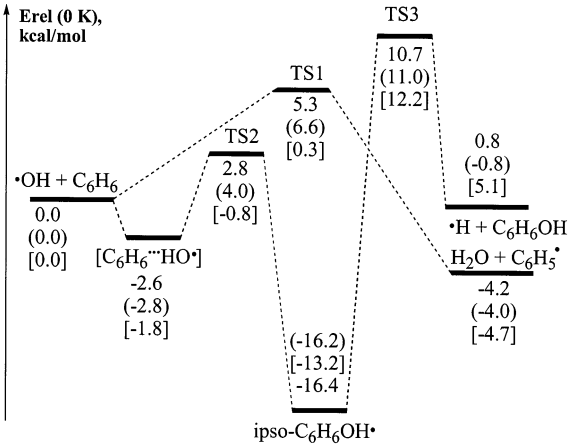

Figure 1. Potential energy diagram for the OH + C_6H_6 reaction calculated at the G3, G2M (in parentheses), and B3LYP/(II) [in square brackets] levels of theory.

It is worth noting that we have previously investigated at the same level of theory the abstraction of the H atom from benzene by methyl.[51]

$$C_6H_6 + CH_3 \rightarrow C_6H_5 + CH_4 \qquad (4)$$

In contrast to the H abstraction by hydroxyl (reaction 1), reaction 4 is endothermic. Accordingly, the transition state of the H transfer from benzene to CH_3, TS1(CH_3−H−C_6H_5), is closer to products. For instance, the breaking C_6H_5−H bond is 1.382

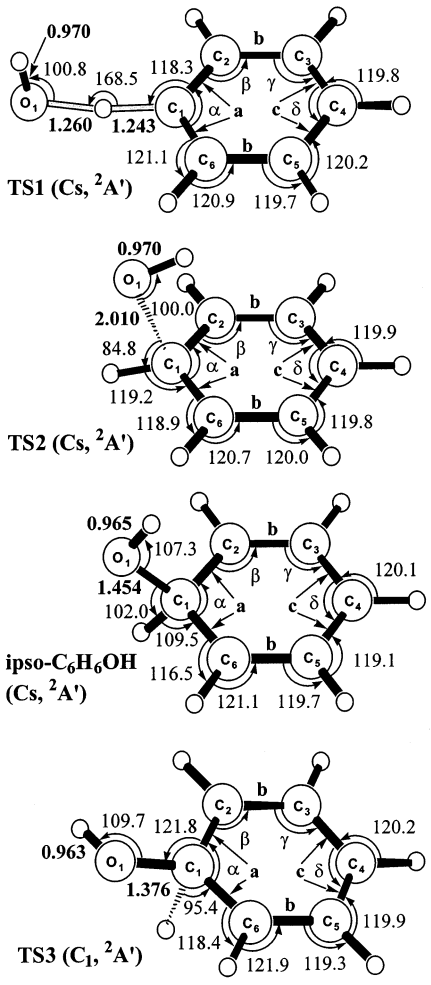

	TS1(X-H-C_6H_5) X = OH	X = CH_3
a	1.385	1.385
b	1.399	1.399
c	1.395	1.395
α	123.3	122.5
β	118.0	118.5
γ	120.1	120.0
δ	120.4	120.3
<C-H>	1.084	1.085

	TS2(X-C_6H_6) X = OH	X = CH_3
a	1.422	1.424
b	1.385	1.385
c	1.401	1.401
α	118.5	117.8
β	120.4	120.4
γ	120.1	120.5
δ	120.3	119.7
(C1-H)	1.081	1.084
<C-H>	1.084	1.084

	ipso-C_6H_6X X = OH	X = CH_3
a	1.501	1.504
b	1.365	1.364
c	1.417	1.417
α	113.1	112.3
β	122.4	122.7
γ	121.2	121.4
δ	119.8	119.4
(C1-H)	1.100	1.106
<C-H>	1.085	1.085

	TS3(H-C_6H_5X) X = OH	X = CH_3
a	1.417	1.416
b	1.385	1.387
c	1.398	1.397
α	118.9	117.4
β	119.7	121.0
γ	120.7	120.3
δ	119.6	119.6
(C1-H)	1.760	1.835
<C-H>	1.084	1.085

Figure 2. B3LYP/6-311++G(d,p)-optimized geometries (bond lengths in angstroms, angles in degrees) of the transition states and intermediate involved in the OH + C_6H_6 reaction. Selected geometric parameters are compared for isoelectronic species involved in the X + C_6H_6 reactions (X = OH, CH_3).

Å in TS1($CH_3-H-C_6H_5$), which is considerably longer than its length of 1.243 Å in TS1($HO-H-C_6H_5$). Nevertheless, the two processes are isoelectronic, and the molecular structures of the H-abstraction transition states by OH and CH_3 radicals have a lot in common. From the comparison of selected geometrical parameters in Figure 2, we found that in these transition states the C_6H_5 units closely resemble each other. Furthermore, judging by the similarity of the expectation values of the $\langle S^2\rangle$ operator for TS1($X-H-C_6H_5$) at both the B3LYP/(II) ($\langle S^2\rangle = 0.76$ for X = OH, CH_3) and UHF/6-311G(d,p) ($\langle S^2\rangle = 1.33$ for X = OH, $\langle S^2\rangle = 1.38$ for X = CH_3) levels of theory, we expect a similar quality of the electronic wave functions for these transition states at different levels of theory and a similar magnitude of theoretical errors in their energies.

The geometry of TS1 optimized by the MPW1K/(I), KMLYP/(I), and MP2/(I) methods is given in Supporting Information. The most significant differences involve the reaction center. Transient values for the breaking C−H and forming O−H bonds are shorter in the MP2/(I)-optimized structure (1.228 and 1.226 Å, respectively). The MPW1K/(I) and KMLYP/(I) methods predict very similar lengths of the breaking C−H bond to that predicted by B3LYP/(II) but a much shorter O−H bond of only 1.223 Å (MPW1K/(I)) and 1.212 Å (KMLYP/(I)). The tighter structure of the TS1 at the KMLYP/(I), MPW1K/(I), and MP2/(I) levels of theory correlates with the higher reaction barriers predicted at these levels and a larger magnitude of the imaginary vibrational frequency (ν_{im}(B3LYP/(II)) = i1193 cm^{-1}, ν_{im}(MPW1K/(I)) = i1664 cm^{-1}, ν_{im}(KMLYP/(I)) = i1775 cm^{-1}, ν_{im}(MP2/(I)) = i2283 cm^{-1}).

TABLE 3: Moments of Inertia[a] (I_A, I_B, I_C), Symmetry Numbers (n), and Vibrational Frequencies[a] of the Intermediates and Transition States

I_A, I_B, I_C/ 10^{-40} g cm^2	sym-metry	frequencies (ν/cm^{-1})[a]
		TS1 ($n = 2$)
150.3, 491.8, 638.6	A′	1193i, 107, 363, 442, 632, 673, 722, 775, 914, 992, 1009, 1030, 1069, 1186, 1245, 1499, 1598, 3162, 3182, 3193, 3766
internal[b] 1.48	A″	100, (118)[b], 405, 612, 827, 972, 1042, 1118, 1181, 1322, 1334, 1468, 1619, 3170, 3188
		TS2 ($n = 1$)
197.8, 332.0, 433.1	A′	327i, 134, 392, 609, 667, 728, 795, 907, 963, 997, 1017, 1031, 1043, 1195, 1484, 1602, 3166, 3185, 3195, 3211, 3766
	A″	132, 188, 405, 610, 836, 984, 1053, 1173, 1181, 1325, 1378, 1496, 1578, 3175, 3196
		$[C_6H_6\cdots OH^{\bullet}]$($C_s$) ($n = 1$)
210.8, 376.7 461.9	A′	74, 135, 414, 475, 619, 683, 710, 875, 982, 999, 1004, 1023, 1051, 1197, 1502, 1624, 3163, 3181, 3192, 3211, 3745
	A″	39, 107, 404, 618, 857, 982, 1059, 1177, 1195, 1334, 1381, 1508, 1613, 3173, 3191
		$C_6H_6OH^{\bullet}$ ($n = 1$)
173.8, 318.2, 452.4	A′	105, 399, 533, 616, 703, 811, 864, 937, 974, 990, 1016, 1192, 1213, 1383, 1450, 1592, 2975, 3156, 3179, 3194, 3796
	A″	283, 355, 442, 584, 756, 971, 1030, 1122, 1170, 1309, 1358, 1411, 1539, 3159, 3179
		TS3 ($n = 1$)
156.0, 328.6, 471.9	A′	951i, 210, 288, 369, 419, 478, 501, 528, 625, 632, 684, 773, 815, 826, 909, 969, 989, 1004, 1035, 1094, 1174, 1184, 1187, 1254, 1338, 1367, 1491, 1508, 1597, 1620, 3160, 3171, 3179, 3194, 3202, 3832

[a] Calculated at the B3LYP/6-311++G(d,p) level. [b] OH torsional rotor.

Other calculated vibrational frequencies of TS1 are tabulated in Table 3 (B3LYP/(II) values) and in Supporting Information (MP2/(I), KMLYP/(I), and MPW1K/(I) values). The OH torsional motion in TS1 is expected to be largely anharmonic. Therefore, we treated it as a 1-D hindered rotor. To estimate the internal rotational barrier V_2(TS1), the planar conformation of TS1 has been optimized on the B3LYP/(II) PES. This conformation is a second-order saddle point with two imaginary frequencies corresponding to the H transfer from benzene to OH and the OH torsional motion. The energy difference of ~0.6 kcal/mol found between the planar and nonplanar C_s symmetric conformations of TS1 is accepted as V_2(TS1). The reduced moment of internal rotation, I_R(TS1) = 1.5 × 10^{-40} g cm^2, has been calculated according to Pitzer and Gwinn[72] with the assumption that the axis of internal rotation passes through the C1 and O atoms.

OH-Addition Channel. The second channel of the OH radical attack on benzene leads to the *ipso*-C_6H_6OH (2,4-cyclohexadienyl, 6-hydroxy) radical, as shown in Figure 1. This radical will preferably decompose back to reactants at higher T via TS2 (reaction −2). Alternatively, it can undergo H elimination to produce phenol via TS3 (reaction 3′). The molecular structures of TS2, *ipso*-C_6H_6OH, and TS3 calculated at the B3LYP/(II) level of theory are illustrated in Figure 2. Next to each structure, selected geometric parameters are compared to

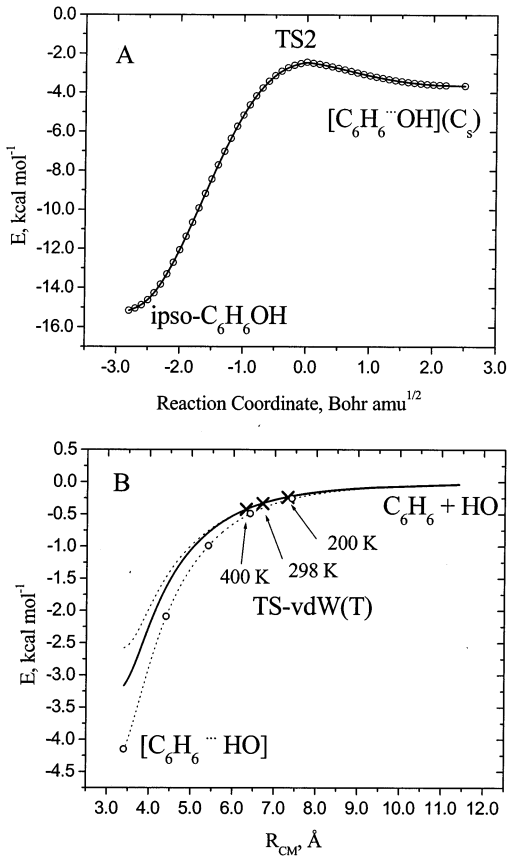

Figure 3. (A) Reaction path following the results from TS2 at the B3LYP/6-311++G(d,p) level of theory. IRC calculations were performed with a step size of 0.1 bohr amu$^{1/2}$. (B) C_6H_6−OH interaction potential calculated at the B3LYP/6-311++G(d,p) (- - -) and G3 levels of theory with (—) and without (○- - -○) BSSE corrections. C_{6v} molecular symmetry was constrained during the PES scan. Effective TS-vdW locations at different T values are designated by ×.

those obtained for the analogous species involved in the H-for-CH_3 exchange process in the reaction of benzene with methyl.[47]

$$C_6H_6 + CH_3 \rightarrow C_6H_6CH_3 \qquad (5)$$

$$C_6H_6CH_3 \rightarrow C_6H_6 + CH_3 \qquad (-5)$$

$$C_6H_6 + CH_3 \rightarrow C_6H_5CH_3 + H \qquad (6)$$

$$C_6H_6CH_3 \rightarrow C_6H_5CH_3 + H \qquad (6')$$

Again we observe very similar geometric transformations in the C_6H_5 units in both H-for-X processes (X = OH, CH_3). The substituent effects are primarily manifested in small variations of valence angles near the reaction center. The $\langle S^2 \rangle$ expectation values at the B3LYP/(II) and UHF/6-311G(d,p) levels are practically identical for isoelectronic species; the largest difference is found for TS3(H−C_6H_5X) at the UHF/6-311G(d,p) level, where $\langle S^2 \rangle = 1.36$ for X = OH and $\langle S^2 \rangle = 1.38$ for X = CH_3.

An important mechanistic difference in the two H-for-X (X = OH, CH_3) exchange processes is found in the OH-addition step. In contrast to the CH_3 addition to benzene and a recently published DFT study of the OH addition to benzene,[23] our detailed IRC calculations for TS2(HO−C_6H_6) did not connect it directly to the reactants but rather to the [C_6H_6···OH]-C_s prereaction complex (see Figure 3A). Its molecular structure is shown in Figure 4. Along the minimum-energy path from TS2 to [C_6H_6···OH]-C_s, the reaction coordinate is mainly associated with the C−O bond separation coupled with small changes in the geometric parameters of the C_6H_6 fragment that bring its structure back to benzene. Apparently, the orientation of OH does not change significantly in this interval. However, a number of stationary points of virtually the same energy as that of the prereaction complex have been located on the PES of the OH addition to benzene, suggesting that the structure of the OH van der Waals complex with C_6H_6 is very flexible with respect to the OH (1,2) and (1,4) shifts (along and across the aromatic ring) and the OH rotation from the parallel to the orthogonal orientation relative to the plane of C_6H_6. The common feature of all of these structures is that the H end of OH is always pointing toward the aromatic ring.

The most symmetric of these stationary points has the OH radical lying on the C_6 axis of symmetry drawn through the center of the benzene ring (see Figure 4). It is characterized by one small imaginary vibrational frequency (ν_{im} = i52 cm^{-1}) corresponding to OH migration across the ring and by four other low-frequency modes (8, 79, 121, and 145 cm^{-1}) that originate from the OH translational and rotational degreees of freedom. The remaining vibrational frequencies of [C_6H_6···HO]-C_{6v} are essentially those of pure benzene and OH; the O−H stretching frequency exhibits the largest shift of −19 cm^{-1}. This batachromic shift is a sign of a weakened O−H bond by the donation of π-electronic density into the antibonding σ*(O−H) MO. However, the magnitude of the frequency shift and the O−H bond elongation (+0.001 Å vs OH) appear to be too small to explain the strength of benzene−OH interactions. We can gain insight into the nature of these interactions by optimizing the entire profile of the OH addition to benzene and looking at the changes in the electronic structure along this profile.

A long portion of the profile is readily available from our IRC calculations for TS2 (Figure 3A). The remaining interval connects the [C_6H_6···OH]-C_s prereaction complex to the reactants. Unfortunately, a straightforward scanning procedure is not applicable for a minimum-energy path optimization in this interval because of the extreme flatness of the PES in the subspace spanned by transitional degrees of freedom. An approximate profile can be obtained if some assumptions about the reaction coordinate are made. At long separations, the reaction coordinate can be reasonably assumed to be the center-of-mass separation (R_{CM}) of the C_6H_6 and OH fragments. Because the OH radical prefers to orient its H end toward the aromatic ring, and taking into account the intrinsic symmetry of the system, the average most-favorable orientation of OH with respect to C_6H_6 will be that of the [C_6H_6···HO]-C_{6v} conformation. Therefore, an approximate profile of the OH addition to benzene at long separations can be obtained with C_{6v} symmetry constraints, and it will be an upper bound to the minimum-energy path.

Figure 3B shows the long-range interaction potential in the interval from [C_6H_6···HO]-C_{6v} to C_6H_6 + OH. The dashed curve was calculated at the B3LYP/(II) level of theory by increasing the R_{CM} separation up to 11.4 Å in steps of 0.1 Å. Then it was scaled to pass through five points computed by G3 theory at the B3LYP/(II)-optimized geometries (dashed curve with circles). For higher accuracy, the calculated interaction potential also has to be corrected for the basis-set superposition error (BSSE). Using the counterpoise method,[73] we evaluated the BSSE correction at the same five points of the G3 potential shown. The magnitude of this correction is 1.0 kcal/mol at the minimum, and it decreases exponentially at longer separations. After including the BSSE correction, the G3 interaction potential (solid

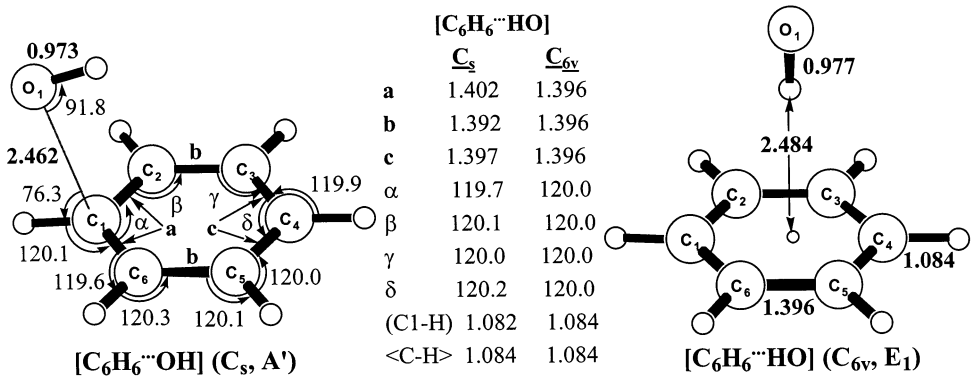

Figure 4. Molecular structure of the $[C_6H_6\cdots OH]$ van der Waals complex. B3LYP/6-311++G(d,p)-optimized geometries of two configurations are shown.

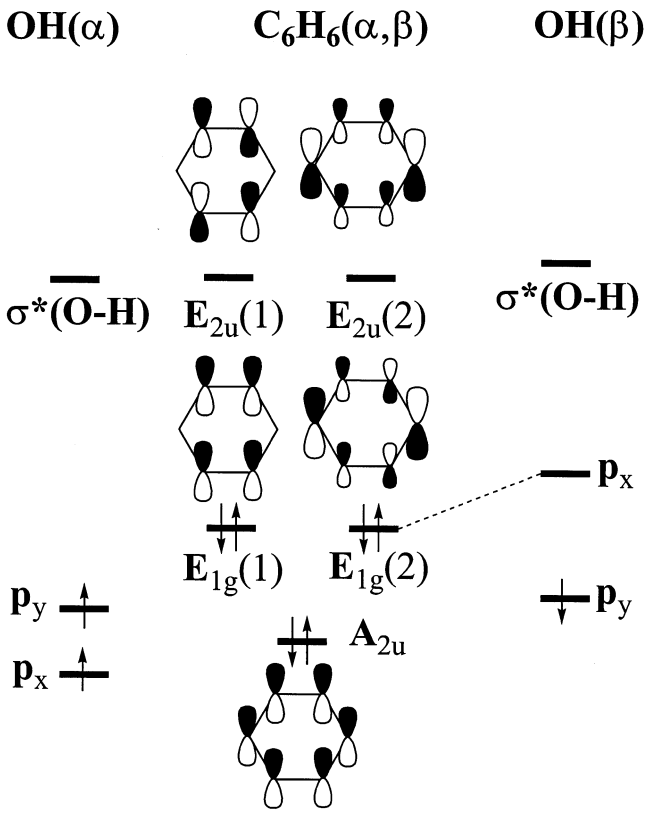

Figure 5. Schematic frontier MO diagram for the C_6H_6 + OH system. The dashed line designates the most important intermolecular MO interaction in the early stages of the OH-addition reaction.

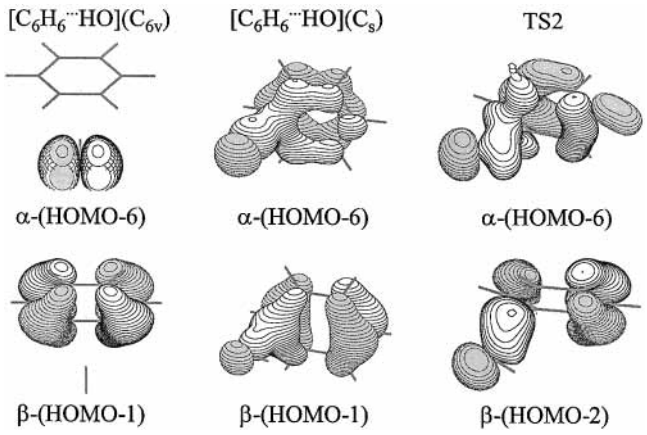

Figure 6. Key molecular orbital interactions between C_6H_6 and OH in the α- and β-spin systems involving the partially occupied p_x orbital of OH.

curve) features a significantly greater well depth than the uncorrected B3LYP potential but coincides with it at long separations. From the shape of the benzene−OH interaction potential, we can see that the strength of attractive interactions slowly decreases with distance so that even at separations greater than 5 Å substantial attraction still exists. This behavior signifies the importance of long-range interactions (electrostatic and dispersion) in the stabilization of the $[C_6H_6\cdots HO]$ van der Waals complex.

Additional stabilization can occur as a result of molecular orbital (MO) overlap. The associated interactions quickly decrease with distance; therefore, they are referred to as short-range interactions. We can gain insight into their nature by tracing the changes in the frontier MOs along the OH-addition profile. Figure 5 shows the initial frontier MO diagram. The π-electronic cloud of benzene is represented by A_{2u} and a pair of E_{1g} MOs; its σ-electronic density is spatially separated from the OH radical. Applying an unrestricted formalism to the OH radical, we obtain different sets of frontier MOs for different spins. The α spin system is represented by a vacant antibonding σ^*(O−H) MO (α-LUMO) and two occupied p orbitals centered on the O atom. We will use *x* and *y* indexes to distinguish between them; the p_x symbol will designate the orbital hosting an unpaired electron (α-HOMO). In the β spin system, only the p_y orbital is occupied (β-HOMO), whereas the other two frontier MOs (p_x and σ^*(O−H)) are vacant (β-LUMO and β-LUMO + 1, respectively).

In the interval from C_6H_6 + OH to $[C_6H_6\cdots HO]$-C_{6v} (Figure 3B), the only nonnegligible MO overlap is found for the σ^*(O−H) + $A_{2u}(C_6H_6)$ combination, but even this interaction is very weak because the energy gap between the MOs involved is too big to allow significant electron density donation from $A_{2u}(C_6H_6)$ to σ^*(O−H). As a result, the molecular structures of the C_6H_6 and OH fragments are subject to very small changes compared to those of pure benzene and OH (see Table 1 and Figure 4).

The nature of benzene−OH interactions changes at smaller separations. A simple frontier MO analysis (Figure 5) identifies the α-p_x + α-A_{2u} and β-p_x + β-$E_{1g}(2)$ interactions as the most important in the α and β spin systems, respectively. The changes in the corresponding MOs are followed along the OH-addition profile in Figure 6. These MOs are not involved in the intermolecular interactions at the $[C_6H_6\cdots HO]$-C_{6v} geometry and beyond because of the large spatial separation. As the molecular symmetry breaks down to C_s and the O atom of OH approaches the benzene ring in the $[C_6H_6\cdots OH]$-C_s structure, the α-p_x orbital of OH overlaps with the energetically closest α-A_{2u} orbital of

TABLE 4: Thermochemical Parameters of Selected Molecules and Radicals Relevant to This Study

species	g_i[a]	$\Delta_f H°_0$, kcal mol^{-1}	$S°_{298}$, cal mol^{-1} K^{-1}	$\Delta_f H°_{298}$, kcal mol^{-1}	ref
hydrogen (H)	2	51.63	27.42	52.10	62
hydroxyl (OH)[b] $^2\Pi_{1/2}$	2	8.86 ± 0.07	43.89	8.92 ± 0.07	75
$^2\Pi_{3/2}$	2				
water (H_2O)	1	−57.10 ± 0.01	45.13	−57.80 ± 0.01	62
methyl (CH_3)	2	35.86 ± 0.07	46.41	35.05 ± 0.07	76
methane (CH_4)	1	−15.99 ± 0.08	44.52	−17.90 ± 0.08	62
methanol (CH_3OH)	1	−45.54 ± 0.05	57.33	−48.16 ± 0.05	74
propene (C_3H_6)	1	8.58 ± 0.1	63.2	4.88 ± 0.1	78
allyl alcohol (C_3H_5OH)	1	−25.6 ± 0.4	69.5	−29.8 ± 0.4	74
phenyl (C_6H_5)	2	84.3 ± 0.6	68.9	81.2 ± 0.6	77
benzene (C_6H_6)	1	23.94 ± 0.15	64.2	19.74 ± 0.15	74
toluene ($C_6H_5CH_3$)	1	17.59 ± 0.15	76.7	12.07 ± 0.15	74
phenol (C_6H_5OH)	1	−18.5 ± 0.2	75.2	−23.0 ± 0.2	74
2,4-cyclohexadienyl (C_6H_7)	2	54.3 ± 2.0	71.9	49.5 ± 2.0	47
2,4-cyclohexadienyl, 6-methyl (*ipso*-$C_6H_6CH_3$)	2	49.1 ± 3.0	80.5	42.9 ± 3.0	47
2,4-cyclohexadienyl, 6-hydroxy (*ipso*-C_6H_6OH)	2	15.8 ± 3.0	79.1	10.6 ± 3.0	this work

[a] Electronic degeneracy. [b] The ground state of the OH radical is split into two spin−orbit components ($^2\Pi_{1/2}$ and $^2\Pi_{3/2}$, Δ = 140 cm^{-1}).

benzene while the β-$E_{1g}(2)$ orbital of benzene donates electronic density into the unoccupied β-p_x orbital of OH. The flow of α electron density from OH's α-p_x orbital and the counterflow of β electron density from benzene's β-$E_{1g}(2)$ orbital into the forming C−O bond become even more apparent in TS2 (see Figure 6). Simultaneously with the C−O bond formation, the uncompensated flows of α and β electron densities described above stipulate a shift of the radical center from the O atom of OH to the carbon atoms of benzene that are not directly involved in the reaction.

The OH-addition profile has been studied in less detail at the MPW1K/(I), KMLYP(I), and MP2/(I) levels of theory. The optimized molecular structures and vibrational frequencies of TS2, *ipso*-C_6H_6OH, and TS3 are given in the Supporting Information. They can be compared to those obtained by the B3LYP/(II) method, which are presented in Figure 2 and Table 3. As in the case of TS1, the MPW1K/(I), KMLYP(I), and MP2/(I) methods predict tighter molecular structures and higher vibrational frequencies. For example, the forming C−O bond in TS2 is 2.010, 1.988, 1.974, and 1.975 Å long according to B3LYP/(II), MPW1K/(I), KMLYP(I), and MP2/(I) predictions, respectively. The corresponding imaginary frequency increases from i327 cm^{-1} (B3LYP/(II)) to i431 cm^{-1} (MPW1K/(I)) to i453 cm^{-1} (KMLYP(I)) to i660 cm^{-1} (MP2/(I)). The imaginary vibrational frequency of TS3 increases in the same order from i951 cm^{-1} to i1039 cm^{-1} to i1040 cm^{-1} to i1495 cm^{-1}, in parallel with the C1−H bond-length decrease from 1.760 Å (B3LYP/(II)) to 1.745 Å (MPW1K/(I)) to 1.736 Å (KMLYP(I)) to 1.660 Å (MP2/(I)).

The vibrational frequency of the OH-torsional motion assumes higher values in TS2, *ipso*-C_6H_6OH, and TS3 than in TS1, which makes a harmonic oscillator approximation suitable for evaluating its contribution to the partition functions, sums, and densities of states.

C. Energetic Parameters and Thermochemistry. Experimental Thermochemistry of the C_6H_6 + OH Reactions and Isodesmic Enthalpy of Formation of the Hydroxycyclohexadienyl Radical. Table 4 contains a compilation of available thermodynamic parameters for various molecules and radicals that appear as reactants or products in reactions 1−6 and in the isodesmic reactions considered in this study. The thermodynamic parameters were adopted from standard reference sources,[62,66,74] except for the hydroxyl, methyl, phenyl, and cyclohexadienyl radicals and propene, for which more accurate values have been established elsewhere.[47,75−78] For those species whose entropies or thermal corrections were not readily available, the missing quantities were evaluated from the theoretical molecular parameters calculated by the B3LYP/(II) method. The thermochemical data calculator included in the ChemRate package[53] was used as a handy tool for such computations.

To assess the stability of the C_6H_6OH radical, we analyzed the following isodesmic reactions:

$$C_6H_6OH + CH_4 \rightarrow C_6H_7 + CH_3OH \quad (7)$$

$$C_6H_6OH + C_3H_6 \rightarrow C_6H_7 + C_3H_5OH \quad (8)$$

$$C_6H_6OH + C_6H_6 \rightarrow C_6H_7 + C_6H_5OH \quad (9)$$

Apart from preserving all bond types, these reactions are also very well balanced with regard to the nature of the open-shell system because each of them has cyclohexadienyl-type radicals on both sides of the equation. Given all these features, the cancellation of errors in the theoretical estimates of the heats of these isodesmic reactions is expected to be nearly complete. Indeed, all predicted values of $\Delta H_{(R)}(0\ K)$ (R = 7, 8, 9) fall in very narrow ranges for each R, as follows from the data presented in Table 5. The predictions are particularly consistent for the heats of reactions 8 and 9. Taking the values obtained by the most accurate G3 method as a base and assuming an accuracy of 0.5 kcal/mol, we arrive at the following estimates of the heats of reactions 7−9 at 0 K: $\Delta H_{(7)}(0\ K) = 9.1 \pm 0.5$ kcal/mol, $\Delta H_{(8)}(0\ K) = 3.9 \pm 0.5$ kcal/mol, $\Delta H_{(9)}(0\ K) = -3.7 \pm 0.5$ kcal/mol.

Then, the heat of formation of the C_6H_6OH radical evaluated by isodesmic reaction analysis can be expressed relative to the heat of formation of the C_6H_7 radical:

$$\Delta_f H_0°(C_6H_6OH) = \Delta_f H_0°(C_6H_7) + \Delta_{H-for-OH} \quad (I)$$

where

$$\Delta_{H-for-OH} = \Delta_f H_0°(CH_3OH) - \Delta_f H_0°(CH_4) - \Delta H_{(7)}(0\ K) \text{ for reaction 7}$$

$$\Delta_{H-for-OH} = \Delta_f H_0°(C_3H_5OH) - \Delta_f H_0°(C_3H_6) - \Delta H_{(8)}(0\ K) \text{ for reaction 8}$$

$$\Delta_{H-for-OH} = \Delta_f H_0°(C_6H_5OH) - \Delta_f H_0°(C_6H_6) - \Delta H_{(9)}(0\ K) \text{ for reaction 9}$$

Combining our calculated heats of isodesmic reactions and available 0 K enthalpies of formation of relevant hydrocarbons and their alcohols from Table 4, we can estimate the correction

TABLE 5: Enthalpy of Formation of the *ipso*-C_6H_6OH Radical from Isodesmic Reaction Analysis

	reaction 7		reaction 8		reaction 9	
computational methods[a]	$\Delta H°_7$(0 K), kcal/mol	$\Delta_f H°_0(C_6H_6OH)$, kcal/mol[b]	$\Delta H°_8$(0 K), kcal/mol	$\Delta_f H°_0(C_6H_6OH)$, kcal/mol[b]	$\Delta H°_9$(0 K), kcal/mol	$\Delta_f H°_0(C_6H_6OH)$, kcal/mol[b]
KMLYP/(I)	8.52	16.24	3.45	16.67	−4.63	16.43
MPW1K/(I)	7.91	16.85	3.25	16.87	−4.66	16.46
B3LYP/(II)	7.89	16.87	3.30	16.82	−4.03	15.89
MP2/6-311G(d,p)[c]	9.85	14.91	4.20	15.92	−3.90	15.76
MP2/6-311+G(3df,2p)[c]	9.18	15.58	3.94	16.18	−3.77	15.63
PMP2/6-311+G(3df,2p)[c]	9.11	15.65	3.87	16.25	−3.84	15.70
MP2(FU)/G3Large[c]	9.19	15.57	3.89	16.23	−4.17	16.03
MP4(SDTQ)/6-311G(d,p)[c]	10.05	14.71	4.40	15.72	−3.60	15.46
PMP4(SDTQ)/6-311G(d,p)[c]	9.93	14.83	4.28	15.84	−3.72	15.58
QCISD(T)/6-31G(d)[c]	9.75	15.01	4.30	15.82	−3.50	15.36
CCSD(T)/6-311G(d,p)[c]	9.51	15.25	4.15	15.97	−3.50	15.36
G2M(CC,MP2)[c]	8.85	15.91	3.89	16.23	−3.37	15.23
G3[c]	9.14	15.62	3.94	16.18	−3.70	15.56

[a] All reaction enthalpies include a ZPE correction calculated at the B3LYP/6-311++G(d,p) level of theory. [b] The 0 K heats of formation of C_6H_6OH are calculated from $\Delta H°_R$(0 K) (R = 7, 8, 9) using eq I. [c] Based on B3LYP/(II) geometries.

term for the H-for-OH substitution in the cyclohexadienyl radical, $\Delta_{H-for-OH}$. Values of −38.6 ± 0.8, −38.1 ± 1.0, and −38.7 ± 0.9 kcal/mol are derived for this correction term from reactions 7, 8, and 9, respectively. The three independent estimates agree very closely so that the weighted mean of −38.5 ± 1.0 kcal/mol can be accepted for $\Delta_{H-for-OH}$. Upon addition of the H-for-OH correction term to the enthalpy of formation of the C_6H_7 radical from Table 4, we obtain $\Delta_f H_0°(C_6H_6OH)$ = 15.8 ± 3 kcal/mol. Corrected to standard conditions, the enthalpy of formation of the *ipso*-C_6H_6OH radical becomes $\Delta_f H_{298}°(C_6H_6OH)$ = 10.6 ± 3 kcal/mol. Then the heat of the OH addition to benzene can be estimated from the enthalpies of formation of the reactants and products as $\Delta H_{(2)}$(0 K) = −17.0±3 kcal/mol and $\Delta H_{(2)}$(298 K) = −18.1 ± 3 kcal/mol. The error range of these estimates is the sum of the theoretical and experimental uncertainties of all thermodynamic parameters used in the isodesmic reaction analysis. Therefore, the actual accuracy of our predictions should be better than 3 kcal/mol. Although all previously determined standard enthalpies of reaction 2 (−16.5 ± 1.4,[10] −18.4 ± 3.1,[6] −18.4 ± 1.4,[8] and −19.9 ± 1.2 [11] kcal/mol) are within a rather conservative error range of our estimate, we suspect that the recommendation of Witte, Urbanik, and Zetzsch[10] may underestimate the exothermicity of reaction 2 (see its criticism in ref 11), whereas the value suggested by Lin, Kuo, and Lee[11] probably overestimates this quantity. The latter value was derived by the third-law method along with the entropy of reaction 2: $\Delta S°_{(2)}$(298 K) = −33.4 ± 2.5 cal/(mol K). A considerably different estimate of $\Delta S°_{(2)}$(298 K) = −29.0 cal/(mol K) follows from our data presented in Table 4. If a smaller value of the entropy of reaction 2 had been used by Lin, Kuo, and Lee, then a higher value of −18.6 kcal/mol for the heat of reaction 2 at RT would have been derived from the third-law method. Berho, Rayez, and Lesclaux[22] obtained an estimate of −17.6 kcal/mol for $\Delta H_{(2)}$(298 K) from the BAC-MP4 calculations; their prediction is in close agreement with ours.

To confirm our estimate of $\Delta H_{(2)}$, we reviewed previous studies of the $C_6H_6 + OH = C_6H_6OH$ equilibrium and extracted the $Kp_{(2)}$ equilibrium constants derived in those studies. The theoretical $Kp_{(2)}$ has been estimated from the B3LYP/(II) molecular parameters of the reactants and product combined with the $\Delta H_{(2)}$(0 K) = −17.0 kcal/mol value obtained from isodesmic reaction analyses. Despite a large difference in the $\Delta H_{(2)}$ values derived by the third-law method by Witte et al.[10] and Lin et al.,[11] the T dependence of the equilibrium constants extracted from both of these studies and from Knispel et al.[17]

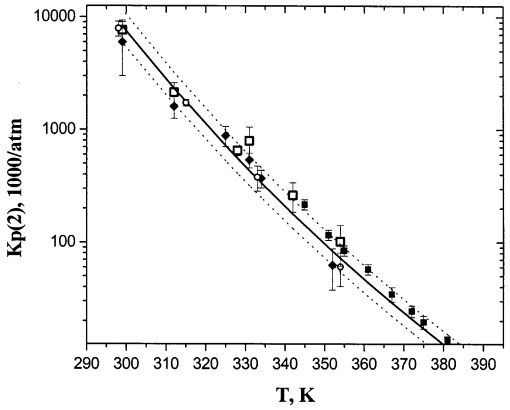

Figure 7. Temperature dependence of the $Kp(2)$ equilibrium constant. The solid line and the two dotted lines represent theoretical values based on the $\Delta H_{(2)}$(0 K) = −17.0 ± 0.2 kcal/mol. Experimental values are taken from Witte et al.[10] ((◆)133 mbar, (□) 200 mbar), Lin et al.[11] (■), and Knispel et al.[17] (○).

agrees remarkably well with our theoretical curve shown in Figure 7. All experimental points can be accounted for by theory with $\Delta H_{(2)}$(0 K) = −17.0 ± 0.2 kcal/mol, which confirms the fact that the actual accuracy of our predicted enthalpy of reaction 2 is better than the 3 kcal/mol stated above.

The thermochemistry of all other reactions relevant to this study is readily available from the thermodynamic parameters of the individual species listed in Table 4. The following experimental enthalpies of reactions have been adopted as benchmarks for examining the performance of various theoretical methods:

$$\Delta H_{(1)}(0\ \mathrm{K}) = -5.6 \pm 0.8\ \mathrm{kcal/mol}$$

$$\Delta H_{(4)}(0\ \mathrm{K}) = 8.5 \pm 0.9\ \mathrm{kcal/mol}$$

$$\Delta H_{(2)}(0\ \mathrm{K}) = -17.0 \pm 3\ \mathrm{kcal/mol}$$

$$\Delta H_{(5)}(0\ \mathrm{K}) = -10.7 \pm 3\ \mathrm{kcal/mol}$$

$$\Delta H_{(3)}(0\ \mathrm{K}) = 0.3 \pm 0.4\ \mathrm{kcal/mol}$$

$$\Delta H_{(6)}(0\ \mathrm{K}) = 9.4 \pm 0.4\ \mathrm{kcal/mol}$$

$$\Delta H_{(-3')}(0\ \mathrm{K}) = -17.3 \pm 3\ \mathrm{kcal/mol}$$

$$\Delta H_{(-6')}(0\ \mathrm{K}) = -20.1 \pm 3\ \mathrm{kcal/mol}$$

On the basis of these enthalpies and theoretical molecular parameters, the equilibrium constants for the major $C_6H_6 + OH$

TABLE 6: Total Energies (ZPE-Corrected, in hartrees) of the Reactants and Relative[a] Energies (in kcal/mol) of the Products, Intermediates, and Transition States for the OH + C_6H_6 Reactions at Various Levels of Theory

species	$OH^\bullet + C_6H_6$	TS1	$H_2O + C_6H_5^\bullet$	$[OH\cdots C_6H_6]^\bullet$ (C_s)[b]	$[OH\cdots C_6H_6]^\bullet$ (C_{6v})[b]	TS2	$C_6H_6OH^\bullet$	TS3	$C_6H_5OH + H^\bullet$
$\langle S^2\rangle$ (UHF/6-311G(d,p))	0.755	1.328	1.377	1.269	0.755	1.396	1.179	1.358	0.750
$\langle S^2\rangle$ (B3LYP/(II))	0.752	0.758	0.757	0.757	0.752	0.781	0.785	0.773	0.750
ZPE (B3LYP/(II))	68.10	65.65	67.90	69.33	68.61	69.75	71.12	66.62	65.24
B3LYP/(I)	−307.89872	−0.11	−4.30	−2.54	−2.15	−1.20	−14.21	11.53	4.61
MPW1K/(I)	−307.79608	5.82	−2.13	(−)	(−)	2.89	−16.57	12.06	3.77
KMLYP/(I)	−307.27154	4.14	−2.19	(−)	(−)	0.58	−21.64	7.47	1.67
MP2/(I)	−306.95068	28.98	16.95	(−)	(−)	27.15	0.85	32.79	−4.07
B3LYP/(II)	−307.96519	0.26	−4.71	−2.42 (−1.83)	−2.07 (−1.64)	−0.79	−13.21	12.16	5.13
MP2/6-311G(d,p)[c]	−307.04205	29.90	19.27	20.64	−3.67 (−2.20)	28.46	1.05	30.38	−4.90
MP2/6-311+G(3df,2p)[c]	−307.22952	28.20	15.11	19.83	−4.06 (−3.06)	26.69	−1.65	27.14	−8.21
PMP2/6-311+G(3df,2p)[c]	−307.23149	6.22	−4.53	2.97	−4.05 (−3.05)	1.77	−16.83	6.06	−6.98
MP4(SDTQ)/6-311G(d,p)[c]	−307.13625	22.61	14.83	13.70	−3.47 (−2.01)	20.14	−4.17	26.70	0.87
PMP4(SDTQ)/6-311G(d,p)[c]	−307.13710	8.93	2.04	−0.80	−3.46 (−2.00)	4.96	−14.75	13.28	1.40
CCSD(T)/6-311G(d,p))[c]	−307.13456	8.29	0.14	1.00	−3.37 (−1.91)	5.77	−13.47	14.25	2.54
G2M(CC,MP2)[c]	−307.42104	6.60	−4.02	0.19	−3.77 (−2.77)	4.00	−16.18	11.01	−0.77
G3[c]	−307.75022	5.25	−4.18	−0.77	−3.64 (−2.64)	2.76	−16.38	10.65	0.81

[a] Energies relative to reactants. [b] BSSE-corrected relative energies are given in parentheses. [c] Based on B3LYP/(II) geometries.

reaction pathways can be estimated over the extended T range of 200−2500 K:

$$K_1 = 130T^{-0.26}\exp(2643/T)$$

$$K_2 = 6.15\times10^{-32}T^{2.00}\exp(9460/T)\ \mathrm{cm^3\ molecule^{-1}}$$

$$K_3 = 5.65\times10^{-7}T^{1.62}\exp(310/T)$$

The expressions of K_1 and K_3 obtained in this work update those of Baulch et al.,[2] which are recommended for combustion modeling. Substantial differences between the old and new values of these equilibrium constants originate from using updated thermochemistry of OH and C_6H_5 in the present work.

Theoretical Energetic Parameters for the C_6H_6 + OH Reactions. The energetic parameters for reactions 1−3 calculated at various levels of theory are presented in Table 6. Potential energy profiles are schematically shown in Figure 1.

In our previous investigations,[47,51] we pointed out systematic theoretical errors in the G2M energetic parameters for reactions of the methyl radical with benzene (reactions 4−6). These errors have been tied to the high spin contamination of the UHF wave function for phenyl and cyclohexadienyl radicals. Our earlier analysis of the molecular structures of the transition states and intermediates involved in reactions 1−3 showed that they closely resemble the isoelectronic structures involved in reactions 4−6. Therefore, qualitatively similar deficiencies in the theoretical energetic parameters can be expected for reactions 1−3 and 4−6. Indeed, the MP2 theory fails to predict the heats of reactions 1, 2, and 3′ by tens of kcal/mol; the perturbation series converge very slowly for those species whose wave functions suffer from high spin contamination (C_6H_5, TS1, TS2, $[C_6H_6^\bullet\cdots OH]$-$C_s$, *ipso*-$C_6H_6OH$, and TS3), much as in the case of reactions 4−6. Even quantitatively, the magnitude of theoretical errors is very similar for analogous reactions. For example, the G2M method underestimates the exothermicity of reactions 1 and 4 by 1.6 and 1.8 kcal/mol,[51] respectively. The same method has an identical error of 1.1 kcal/mol for the heats of reactions 3 and 6. The heat of H addition to benzene and toluene was underestimated by 2.6 kcal/mol at the G2M level;[47] this error is reduced to 1.9 kcal/mol for H addition to phenol at the ipso position (reaction −3′). An exact coincidence of theoretical errors should not be expected for the aforementioned isoelectronic reactions (particularly for such reactions as −3′ and −6′) because of considerable uncertainties in the benchmark values of the reaction enthalpies.

On the basis of the comparison of the G2M(CC,MP2) and G3 energetic parameters, we conclude that G3 theory performs better for the present system and that it provides the most accurate thermochemistry for reactions 1−3 among all the methods employed in our study. The largest error of 1.4 kcal/mol is found in the G3 prediction of $\Delta H_{(1)}$(0 K); all other reaction enthalpies deviate from the benchmark values by less than 0.6 kcal/mol, which means that they are within the uncertainty of the experimental values.

An accurate prediction of reaction barriers from first principles is a more difficult task than the estimation of reaction enthalpies because an equally good performance of the theoretical method is now required for both the equilibrium and transient structures. Because of the intrinsic difficulty of an accurate treatment of electron correlation away from equilibrium geometries, even highly correlated methods such as CCSD(T) or QCISD(T) with insufficiently large basis sets may not recover a significant part of the correlation energy. In our earlier experience,[47] the G2M barriers had to be scaled down by as much as 3.5 kcal/mol in order to account for the experimental activation energies of the H-atom addition to benzene and toluene. The estimates provided by G3 theory surpass in quality those obtained by the G2M method not only for reaction enthalpies but for barriers as well. The G3 reaction barriers are systematically lower than the G2M values; the improvement is as much as 1.9 kcal/mol for the barrier of H addition to phenol (reaction −3′).

Figure 1 compares other relative energies obtained at the G3 and G2M levels of theory to each other and to the B3LYP/(II) values. For the present system, the B3LYP energetic parameters are the least reliable among those of the three methods. This can be illustrated for the present system by the enthalpy of reaction 3, which is overestimated by 4.8 kcal/mol at the B3LYP/(II) level. Furthermore, this density functional typically underestimates barrier heights, as in the case of both OH-addition and H-abstraction transition states. That is why B3LYP energetic parameters cannot give reliable estimates of the rate constants and branching ratios for competing channels in the reaction of the OH radical with benzene.

The formation of the relatively stabilized van der Waals complex of the OH radical with benzene is an important step in the OH-addition pathway. Previous theoretical investigations

of the mechanism of OH addition to ethylene[79−82] concluded that the formation of the [C_2H_4···OH] prereaction complex explains an apparently negative activation energy for that reaction. The ability of B3LYP theory to describe OH radical addition reactions in general and molecular structures of prereaction complexes in particular was questioned in two of those studies.[81,82] Consequently, the authors favored optimization by the MP2 method with large basis sets. The reported results on the use of B3LYP theory were somewhat controversial,[82] in part because of the intrinsic difficulty of geometry optimization of very flexible structures and the incompleteness of the PES. In our opinion, the molecular structures of various species optimized by the B3LYP/(II) method in the present study are reasonable. However, the lowest-energy configuration of the [C_6H_6···OH] prereaction complex remains to be confirmed experimentally or at higher levels of theory.

As alluded to above, we have studied two conformations of the [C_6H_6···OH] van der Waals complex in detail (Figure 4). The C_{6v}-symmetric structure lacks significant interfragment MO overlap, and it is relatively well described by different methods. Long-range attractive forces play the most important role in the stabilization of this structure. The most accurate estimates of the stabilization energy are given by G3 and G2M methods in the amount of 2.6−2.8 kcal/mol. These estimates include ZPE and BSSE corrections. A highly correlated level of theory is needed to evaluate attractive dispersion interactions between the two fragments in the complex accurately. HF and density functional theories lack this capability; as a result, the stabilization energy of the [C_6H_6···OH]-C_{6v} complex is underestimated by the B3LYP/(II) method (see Table 6.).

All post-SCF methods have problems in accurately describing the electronic structure of the C_s-symmetric form of the [C_6H_6···OH] prereaction complex, which is reflected in an abnormally high expectation value of the $\langle S^2 \rangle$ operator for the UHF wave function of [C_6H_6···OH]-C_s. Only G3 theory places this complex below the reactants. Clearly, the stabilization energy of the [C_6H_6···OH]-C_s complex is considerably underestimated even at high levels of theory such as G2M and G3. With such deviations, no definite conclusion can be drawn with respect to whether the [C_6H_6···OH]-C_s structure really corresponds to the minimum of the C_6H_6 and OH intermolecular potential or whether it is just an artifact of the B3LYP method. Regardless of the nature of this structure, we estimate the stabilization energy of the [C_6H_6···OH] van der Waals complex to be ≥2.6 kcal/mol (ΔH_{vdW}(0 K) ≤ −2.6 kcal/mol) on the basis of the G3 energy for [C_6H_6···OH]-C_{6v}. Interestingly, the binding of OH to C_6H_6 is stronger than that to C_2H_4 in this stage of the van der Waals complex formation, but the final heat of OH addition to benzene is much smaller than that in the reaction with ethylene. This is a direct consequence of the different nature of binding interactions at different intermolecular separations (the stability of the prereaction complexes is determined by the strength of electrostatic and dispersion interactions, whereas the stability of the OH-addition products depends on the strength of the C−O chemical bonds).

In conclusion of this section, we briefly examine the PMP2, MPW1K, and KMLYP energetic parameters. According to Sekusak, Leidl, and Sabljic,[81] the annihilation of admixtures of unwanted spin states by means of the projection operator significantly improves the energies of the open-shell species involved in the OH reaction with ethylene. The PMP2 method with large basis sets was recommended as the most reliable method, surpassing G2 and CCSD(T) theories with triple-ξ-quality basis sets. For the present C_6H_6 + OH system, the quality of PMP2/6-311+G(3df,2p) reaction barriers and enthalpies is comparable to the G2M and G3 predictions, with the exception of $\Delta H_{(3)}$(0 K), which is underestimated by more than 7 kcal/mol. The MPW1K and KMLYP density functionals provide more realistic barriers than B3LYP. In particular, the KMLYP/(I) method predicts very accurate barriers for reactions 1 and 2 (vide infra). However, the enthalpies of reaction 1 calculated by these methods deviate from the experimental value by more than 3 kcal/mol. In addition, the KMLYP/(I) model considerably overestimates the exothermicity of the H- and OH-radical addition to aromatic substrates (reactions 2 and 3′), whereas the MPW1K/(I) method gives a poor prediction of the $\Delta H_{(3)}$(0 K) value. Deviations in excess of 3 kcal/mol in the reaction enthalpies disqualify the MPW1K and KMLYP density functionals from being recommended for the elucidation of reliable energetic parameters for the C_6H_6 + OH system. Nevertheless, we selected these methods, along with G2M and G3 theories, as sources of energetic parameters for rate-constant calculations. By comparison with available experimental kinetic data, we will derive the scaling factors for theoretical barriers and discuss the predictive power of the best theoretical estimates.

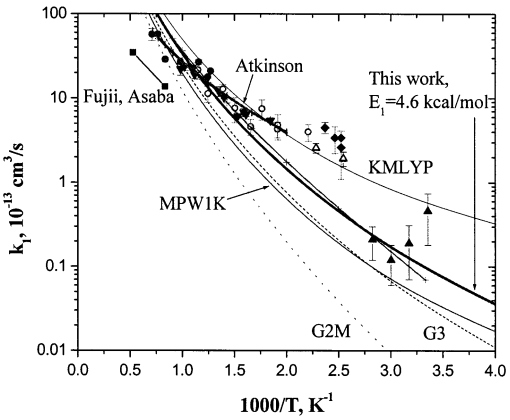

Figure 8. Arrhenius plot of the rate constant for the OH + C_6H_6 = H_2O + C_6H_5 reaction. Four theoretical curves are calculated by conventional TST with Eckart tunneling corrections based on MPW1K/(I), KMLYP(I), G2M//B3LYP(II), and G3//B3LYP(II) molecular and energetic parameters. The recommended rate constant is based on the reaction barrier of E_1(0 K) = 4.6 kcal/mol. Literature values are taken from Atkinson[3] (−|−|−), Knispel et al.[17] (−×−×−, ▲), Fujii and Asaba[4] (■), Madronich and Felder[5] (●), Tully et al.[7] (▼), Lorenz and Zellner[8] (○), Wallington et al.[9] (△), and Perry et al.[6] (◆).

D. Rate-Constant Calculations. C_6H_6 + OH → C_6H_5 + H_2O. The H-abstraction mode (reaction 1) dominates in the OH radical reaction with benzene at elevated temperatures. The available experimental kinetic data pertinent to reaction 1 is presented in Figure 8. Atkinson[3] applied a unit-weighted least-squares analysis to the combined data of Felder and Madronich,[5] Tully et al.,[7] and Lorenz and Zellner[8] to obtain the recommendation of $k_1 = 4.67 \times 10^{-18} T^2 \exp(-543/T)$ cm^3/s at T = 453−1409 K. The preferred values of Baulch et al.[2] ($k_1 = 2.7 \times 10^{-16} T^{1.42} \exp(-732/T)$ cm^3/s) differ by less than 25% from those suggested by Atkinson and are not shown in Figure 8 to avoid clutter. Wallington et al.[9] studied the C_6H_6 + OH reaction at 393 and 438 K and concluded that the abstraction channel still dominates even at these lower temperatures. The total rates of the C_6H_6 + OH reaction measured by Wallington et al.[9] are in good agreement with Atkinson's recommended values of k_1 extrapolated to lower T, whereas the rate constants obtained under similar conditions by Perry et al.[6] are up to 2 times higher. According to Tully et al.,[7] the OH-addition channel may still contribute to the total rate up to $T \approx$ 450 K. Further

support for this opinion can be found in the study of Lin, Kuo, and Lee,[11] who concluded that the H-abstraction channel is negligible at T as high as 385 K (k_1(385 K) < 0.5×10^{-13} cm^3 molecule^{-1} s^{-1}). Clearly, this conclusion is in contradiction with the k_1(393 K) value of 1.9×10^{-13} cm^3 molecule^{-1} s^{-1} reported by Wallington et al.,[9] which makes the interpretation of the kinetic data of Wallington et al.[9] and Perry et al.[6] in terms of the abstraction mechanism alone questionable. The validity of the extrapolation of the high-T expression for k_1 to ambient T is questionable because much lower values of k_1 have been derived by Knispel et al.[17] from modeling the OH decays at low T (298−374 K). The latter rate constants, however, have a relatively large scatter and uncertainty and should be taken cautiously. Nevertheless, Knispel et al.[17] used them in combination with the high-T data of Tully et al.[7] to obtain an improved expression of $k_1 = 1.89 \times 10^{-17} T^2 \exp(-1650/T)$ cm^3/s over an extended T range of 298−1050 K. The discrepancy between the k_1 values recommended by Knispel et al. and Atkinson's high-T expression of k_1 extrapolated to low T reaches 1 order of magnitude at RT.

We have applied the canonical transition-state theory with unsymmetric Eckart tunneling corrections[51,83] to evaluate the k_1 rate constant from theoretical molecular and energetic parameters (Tables 2, 3, 6). The calculated rate constants are plotted in Figure 8. As we mentioned in the previous section, reaction barriers are likely to be overestimated by G2M theory. As a result, the G2M rate constants are consistently lower than the experimental values. At this level, the theoretical barrier needs to be lowered by 2 kcal/mol for the calculated rate constants to approach the recommended values of Knispel et al.[17] Such an adjustment is qualitatively and quantitatively similar to the well-established G2M errors of 1.5−2.0 kcal/mol in the enthalpies of the H-abstraction reactions from benzene by H,[84] CH_3,[51] and OH radicals. These errors result from the poor performance of the G2M theory for the phenyl radical, hence the overestimated C−H bond strength in C_6H_6.[84] A larger downward shift of ∼3.1 kcal/mol has to be applied to the G2M barrier for reaction 1 to account for low-T rate constants extrapolated from the k_1 expressions recommended by Atkinson[3] and Baulch et al.[2] Even after such an adjustment, the calculated rate constant fits recommended values at low T but overestimates the more-reliable high-T reference data. We also believe that the error in the G2M barrier for reaction 1 is unlikely to exceed 3 kcal/mol. Therefore, we tentatively assign a value of 4.6 kcal/mol (the G2M value lowered by 2 kcal/mol) to the barrier of reaction 1 at 0 K. After this adjustment, the rate constant calculated from the B3LYP/(II) molecular parameters for reaction 1 is best expressed in the following form: $k_1 = 6.70 \times 10^{-22} T^{3.33} \exp(-732.4/T)$ cm^3 molecule^{-1} s^{-1} (T = 200−2500 K). The expression of k_1 recommended by Knispel et al.[17] agrees very well with the latter theoretical estimate.

As expected, the rate constants calculated from the G3//B3LYP/(II) energetic and molecular parameters are in better agreement with experimental values than the G2M rate constants discussed above, but the reaction barrier is still likely to be overestimated at this level. The rate constants calculated from the molecular and energetic parameters obtained with the MPW1K density functional are very close to the G3-based estimates. The major difference is a stronger curvature of the Arrhenius plot at low T. On the basis of the magnitude of imaginary frequencies (ν_{im}(B3LYP/(II)) = i1193 cm^{-1}, ν_{im}(MPW1K/(I)) = i1664 cm^{-1}), the barrier for reaction 1 is substantially narrower at the MPW1K/(I) level of theory, which explains the larger enhancement of the MPW1K rate constants by quantum mechanical tunneling at low T. Tunneling corrections of a similar magnitude apply to the rate constants calculated from the KMLYP/(I) molecular and energetic parameters. These rate constants are very close to the values reported by Wallington et al.[9] and to Atkinson's high-T expression of k_1 extrapolated to low T.[3] The agreement, however, becomes worse at high T. As alluded to above, similar rate constants can be obtained from B3LYP/(II) molecular parameters and an assumed reaction barrier of 3.5 kcal/mol. However, we believe the extrapolation of the high T expressions of k_1 to low T is not reliable (i.e., KMLYP method overestimates the k_1 values both at high and low T).

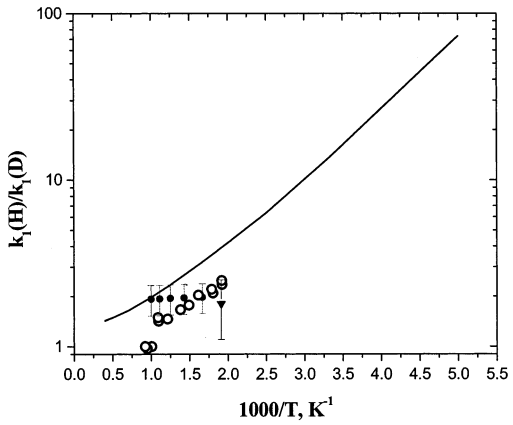

Figure 9. Kinetic isotope effect in the OH + C_6H_6 = H_2O + C_6H_5 reaction. Our prediction (−) is compared to the reported values of Tully et al.[7] (●), Lorenz and Zellner[8] (▼), and Mulder and Louw[16] (○).

Complementary experimental kinetic data for a reverse reaction of the phenyl radical with water would be very valuable for establishing the low-T kinetic parameters with more confidence. Unfortunately, no direct experimental measurement of the rate of reaction −1 is available. Madronich and Felder[5] recommended a value of $k_{-1} = (1.0 \pm 0.3) \times 10^{-14}$ cm^3/s at $T \approx 1310$ K. Using their measured value of k_1(1309 K) = $(5.74 \pm 0.34) \times 10^{-12}$ cm^3/s, we arrive at the estimate of the equilibrium constant K_1(1310 K) = 574 ± 200. This value is in poor agreement with our calculated value of K_1(1310 K) = 160 ± 50, which is based on the experimental value of $\Delta H_{(1)}$(0 K) = −5.6 ± 0.8 kcal/mol and theoretical molecular parameters of the reactants and products calculated by the B3LYP/(II) method. The calculated equilibrium constant should be very reliable since the thermochemistry of reaction 1 is well established and the replacement of theoretical molecular parameters with available experimental moments of inertia and vibrational frequencies changes K_1 by less than 10% at any given T.

Another quantity that can be estimated very reliably is the kinetic isotope effect k_1(H)/k_1(D) for H versus D abstraction from benzene. Although our predicted absolute barrier for reaction 1 may not be very accurate, the k_1(H)/k_1(D) ratio is not sensitive to it because only the relative height of TS1(D) versus TS1(H) is important. The barrier for the C_6D_6 + OH = C_6D_5 + HOD reaction is 1.17 kcal/mol higher than that for reaction 1, as follows from the differences in ZPE corrections for C_6H_6, C_6D_6, TS1(H), and TS1(D) calculated by the B3LYP/(II) method. This is the main factor that influences the k_1(H)/k_1(D) ratio. The second most-important factor is due to quantum mechanical tunneling, which further increases the k_1(H)/k_1(D) ratio at low T. Therefore, the predicted kinetic isotope effect has a strong T dependence, as illustrated in Figure 9.

Only a few studies reported the measured values of $k_1(H)/k_1(D)$. Our calculation agrees only with the high-T data of Tully et al.[7] In contrast to our prediction, the kinetic isotope effects measured by Tully et al.[7] and Lorenz and Zellner[8] do not increase at low T but remain constant with $k_1(H)/k_1(D) \leq 2$ over the range of $T = 520-1000$ K. The uncertainty of these experimental kinetic isotope effects is relatively large because the measurements were made separately for $k_1(H)$ and $k_1(D)$. Strictly speaking, only the total rates of the $C_6H_6 + OH$ and $C_6D_6 + OH$ reactions were measured and ascribed to be the abstraction rates. Contributions from other reactions, such as those involved in the OH-addition channel, would lower the observed kinetic isotope effects at lower T. This could be the reason for their deviation beyond the error limits from the theoretical curve at $T < 800$ K. The deviation of the kinetic isotope effects measured by Tully et al.[7] and Lorenz and Zellner[8] from the theoretical predictions for reaction 1 is another reason to doubt the accuracy of previously reported rate constants below 800 K.

Mulder and Louw[16] derived much different kinetic isotope effects from the competitive measurements of phenol production in the $OH + C_6H_6/C_6D_6$ reactions. Their data has the correct T dependence but systematically underestimates the $k_1(H)/k_1(D)$ ratio by 30−40%. The accuracy of these values is expected to be superior to the results of Tully et al.[7] and Lorenz and Zellner[8] because they were derived from product analyses of the competing $OH + C_6H_6/C_6D_6$ reactions. However, the validity of attributing the measured kinetic isotope effects to the $k_1(H)/k_1(D)$ ratio depends on reaction 1 being the rate-determining step in the complex mechanism of phenol formation in the presence of O_2 and other compounds. Phenol yields of ~25% have been reported under tropospheric conditions,[27−29] where reaction 1 is far less important than the OH-addition channel. Therefore, reaction 1 cannot be responsible for the low-T phenol formation, and it may not be the only pathway from benzene to phenol at high T. If other reactions (such as $C_6H_6 + O(^3P)$ or $C_6H_6OH + O_2 \rightarrow C_6H_5OH + HO_2$) can contribute to the formation of phenol or to its isotopically selective removal (such as $C_6H_5OH/C_6D_5OH + OH/O(^3P)/O_2$), that would explain the systematic underestimation of the $k_1(H)/k_1(D)$ ratio in the experiments of Mulder and Louw.[16]

OH-Addition Channel. The mechanism of the $OH + C_6H_6$ reaction under atmospheric conditions is dominated by the OH-addition channel, which has been typically described by a model including reactions 2, −2, and 3′ as elementary steps. According to our theoretical findings, a more accurate model can be proposed that breaks reaction 2 into two elementary steps, namely, the initial formation of the $[C_6H_6\cdots HO]$ prereaction complex followed by its isomerization to the *ipso*−C_6H_6OH radical:

$$\begin{array}{ccccccc} C_6H_6 + OH & \overset{\text{TS-vdW}}{\rightleftharpoons} & [C_6H_6...HO]^* & \overset{(M)}{\rightleftharpoons} & [C_6H_6...HO] & (k_{vdW}) \\ & & \Downarrow \text{TS2} & & & & \\ (k_3)\ C_6H_5OH + H & \overset{\text{TS3}}{\longleftarrow} & C_6H_6OH^* & \overset{(M)}{\rightleftharpoons} & C_6H_6OH & (k_2) \end{array} \qquad \text{(II)}$$

This model would be more realistic if various radical-loss reactions (diffusion of R out of the reaction zone, loss due to collisions with the reactor walls, and side reactions of R with other radicals and molecules, where R = OH, $[C6H_6\cdots OH]$, and C_6H_6OH) were included. However, these processes are specific to a given experimental setup and cannot be accurately quantified a priori. That is why we assume in our model that the radical-loss reactions can be neglected. Therefore, our proposed mechanism of the OH-addition channel involves only chemical activation, reversible isomerization, collisional stabilization, and decomposition reactions, as depicted in reaction scheme II.

The chemical activation channel is variational for the present system because the TS-vdW is not clearly defined on the potential energy profile (see Figure 3B). Furthermore, the molecular structure in the transition region is very flexible with respect to internal rotations of the C_6H_6 and OH fragments. A suitable approach to evaluate the k_{vdW} rate constant is given by canonical flexible transition-state theory (FTST):[85]

$$k_{vdW}(T) = g_e \frac{1}{\beta h} \frac{\sigma}{\sigma^\dagger} \frac{\exp(-\beta E^\dagger_{TS-vdW})}{Q_{trans}(T)} \frac{Q^\dagger_v(T)}{Q_{v,C_6H_6}(T)\, Q_{v,OH}(T)} \times \frac{Q^\dagger_{pd}(T)\, Q^\dagger_{r,C_6H_6}(T)\, Q^\dagger_{r,OH}(T)}{Q_{r,C_6H_6}(T)\, Q_{r,OH}(T)} \Gamma^\dagger(T) \qquad \text{(III)}$$

At long separations, the molecular structures of the C_6H_6 and OH fragments are virtually the same as for the reactants, resulting in the cancellation of electronic, external rotational, and vibrational partition functions. To a first approximation, the hindering function $\Gamma^\dagger(T)$ is equal to 1 (i.e., the internal rotation is free). Then the simplified expression of k_{vdW} is obtained as follows:

$$k_{vdW}(T) \approx \frac{1}{\beta h} \frac{\exp(-\beta E^\dagger_{TS-vdW})}{Q_{trans}(T)} Q^\dagger_{pd}(T) \qquad \text{(IV)}$$

where

$$Q^\dagger_{pd}(T) = \frac{8\pi^2 \mu R_{CM}{}^2}{\beta h^2} \qquad Q_{trans}(T) = \left(\frac{2\pi\mu}{\beta h^2}\right)^{3/2} \qquad \beta = \frac{1}{k_B T}$$

The R_{CM} distance used in the calculation of the pseudo-diatomic rotational partition function $Q^\dagger_{pd}$ is the separation of the centers of mass of the two fragments, at which the minimum of the k_{vdW} rate constant is located at a given temperature T. $E^\dagger_{TS-vdW}$ is the effective barrier equal to the potential energy of the C_6H_6 and OH fragments separated by R_{CM}. At any separation, the $E^\dagger_{TS-vdW}(R_{CM})$ value is negative because it is defined relative to the reactants. We found that the effective TS-vdW location varies with T as illustrated in Figure 3B (BSSE-corrected G3 interaction potential was used for FTST calculations). Therefore, for each T, we defined specific molecular and energetic parameters for the effective TS-vdW. For all other TSs and stable species, we used T-independent molecular parameters given in Tables 2 and 3.

Note that $k_{vdW}[C_6H_6][OH]$, where k_{vdW} is given by eq III or IV, is the total rate of chemical activation, which is not corrected for the decomposition of a fraction of active molecules back to the reactants. This fraction is determined by an interplay of association, isomerization, decomposition, and stabilization channels (see scheme II), which in turn is governed by the master equation.[55] To calculate P-, T-, and t-dependent effective rate constants that can be related to those derived from experimental studies, we carried out weak collision master equation/RRKM modeling with the help of the ChemRate program.[53]

Realizing that some critically important theoretical input parameters, such as reaction barriers, are not accurately known, we tried to deduce their values by analyzing the most-reliable experimental kinetic data. The high-pressure limiting (HPL)

value of the effective total rate constant $k^{\infty}_2(298\ \mathrm{K}) = 1.4 \times 10^{-12}$ cm^3 molecule^{-1} s^{-1} has been recommended by Atkinson,[3] and it is supported by the majority of experimental studies. Our test rate-constant calculations showed that at RT and high P (P > 100 mbar) the total rate of the C_6H_6 + OH reaction is most sensitive to the 0 K energy of TS2 relative to that of the reactants. We will designate this parameter as E_2.[86] When using the G3 value of E_2 = 2.8 kcal/mol, the calculated k^{∞}_2 rate constant is more than 1 order of magnitude below the experimental value. However, the k^{∞}_2 rate constant is considerably overestimated at low T if the B3LYP/(II) value of $E_2 = -0.8$ kcal/mol is used. A fitted value of $E_2 = 0.1 \pm 0.1$ kcal/mol allows us to account for the experimental $k^{\infty}_2(298\ \mathrm{K})$ value.

After accepting the $E_2 = 0.1$ kcal/mol value in our final rate constant calculations based on B3LYP/(II) molecular parameters, we were able to reproduce closely the experimentally observed effects of P and T on the rate of reaction 2 (vide infra). Apparently, the closest theoretical estimate of E_2 is obtained with the KMLYP density functional, which overestimates the fitted value by 0.5 kcal/mol. The G2M and G3 barriers have to be lowered (by ~3.9 and ~2.7 kcal/mol, respectively) to account for the measured rates of the C_6H_6 + OH reaction. Although the corrections are substantial, they reasonably agree with an error of 3.5 kcal/mol previously found[47] in the G2M barriers of simpler radical additions to aromatics (H + C_6H_6/$C_6H_5CH_3$).

Similar theoretical errors are expected in the G2M and G3 estimates of E_3, the relative energy of TS3. By analyzing the experimental kinetic data for the C_6H_5OH + H reaction (see Appendix 1), we estimated the 0 K barrier for H addition to phenol at the ipso position to be $E_{(-3)} = 8.0 \pm 0.5$ kcal/mol, which converts into $E_3 = \Delta H_{(3)}(0\ \mathrm{K}) + E_{(-3)} = 8.3 \pm 0.9$ kcal/mol. However, even after lowering the E_3 value to 7.4 kcal/mol, the H-elimination branch 3′ makes a negligibly small contribution to the total rate of the C_6H_6 + OH reaction so that it could be safely neglected in our rate-constant calculations for the OH-addition channel at T < 400 K.

Summarizing the preceding discussion, the following energetic parameters have been adopted in our final rate-constant calculations for the OH-addition channel: $E^{\dagger}_{\mathrm{TS-vdW}}$ varies with T ($E^{\dagger}_{\mathrm{TS-vdW}} = -0.25 - 0.42$ kcal/mol for calculations at T = 200−400 K); $\Delta H_{\mathrm{vdW}}(0\ \mathrm{K}) = -2.6$ kcal/mol; $E_2 = 0.1$ kcal/mol; $\Delta H_{(2)}(0\ \mathrm{K}) = -17.0$ kcal/mol, $E_3 = 8.3$ kcal/mol; $\Delta H_{(3)}(0\ \mathrm{K}) = 0.3$ kcal/mol. In the following section, the effects of P, T, and reaction time t on the apparent rate of the OH-radical addition to benzene will be evaluated and compared to the experimental observations.

A strong P dependence of the apparent rate of the OH addition to benzene has been reported at RT below P = 10 mbar.[8,10,18,34−36] Figure 10 illustrates the effects of P and the bath gas on the apparent rate constant k_2. Its falloff behavior is primarily determined by the magnitude of the $\langle\Delta E\rangle_{\mathrm{down}}$ parameter (average energy loss per collision) used in the calculation of the energy-transfer probabilities. Values of $\langle\Delta E\rangle_{\mathrm{down}}$ were obtained by fitting the experimentally observed P dependencies, and they amounted to 150 ± 30 cm^{-1} for He and 400 ± 100 cm^{-1} for Ar. The uncertainties in these estimates are very large because the P dependence was measured over a relatively narrow range and with large scatter. Nevertheless, simulated rate constants accurately reproduce the experimental falloff behavior observed by Lorenz and Zellner[8] and by Witte et al.[10] in Ar and by Goumri et al.[18] in He. The P-dependent rate constants reported by Davis et al.[34] are systematically higher. Helium was used as a bath gas in the latter study. However, the rate constants obtained by Davis et al.[34] considerably exceed all other reported

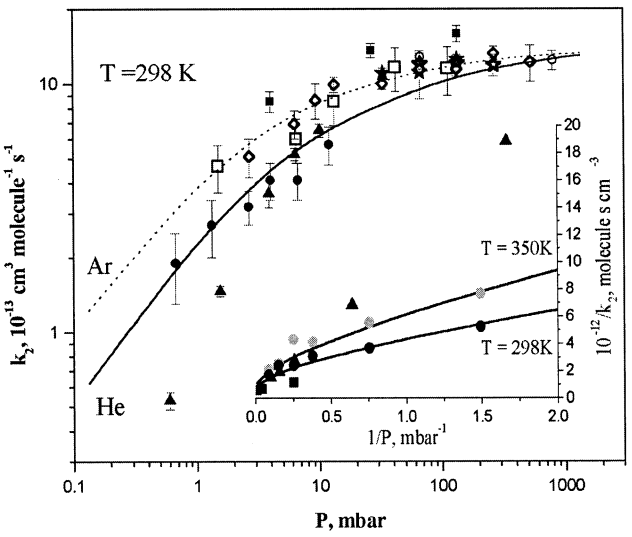

Figure 10. Main plot: P-dependence of the apparent rate constant for the OH addition to benzene at RT. Inset: Lindemann plot of the same rate constant at 298 and 350 K with bath-gas He. Experimental data: Goumri et al.[18] (●), Baulch et al.[35] (▲), Davis et al.[34] (■), Witte et al.[10] (◇), Lorenz and Zellner[8] (□), Tully et al.[7] (★ in He, ☆ in Ar), Hansen et al.[36] (○). Theoretical curves are obtained from ChemRate calculations using the kinetic model described in the text and the following energy-transfer parameters: $\langle\Delta E\rangle_{\mathrm{down}}$(He, 298 K) = 150 cm^{-1}; $\langle\Delta E\rangle_{\mathrm{down}}$ (He, 350 K) = 220 cm^{-1}; $\langle\Delta E\rangle_{\mathrm{down}}$ (Ar, 298 K) = 400 cm^{-1}; Lennard-Jones parameters: σ(He) = 2.55 Å, ϵ(He) = 10.2 K, σ(Ar) = 3.54 Å, ϵ(Ar) = 93.3 K, $\sigma(C_6H_7O)$ = 4.50 Å, and $\epsilon(C_6H_7O)$ = 450 K, as adopted from phenol.[59] Reaction time: t = 1 ms.

values at the same P, including those measured in Ar, which is in sheer contradiction with the expected bath-gas effect. The two lowest P points of Baulch et al.[35] cannot be accounted for by theory with a reasonable value of $\langle\Delta E\rangle_{\mathrm{down}}$ either. In the inset of Figure 10, we provide another view of the P-dependent rate constants measured in He by plotting the inverse rate constant versus inverse pressure (Lindemann plot). The data of Baulch et al.[35] exhibits an unexpected linear dependence with a very steep rise at low P. Therefore, among all of the reported effects of P on the apparent rate of reaction 2 in He, our calculation reasonably agrees only with the data of Goumri et al.[18]

The latter study was the only one that also provided the P-dependent rate constants at other than RT. As shown in the inset of Figure 10, the rate constants measured at 350 K can be closely modeled with $\langle\Delta E\rangle_{\mathrm{down}} \approx 220$ cm^{-1}, suggesting that this parameter strongly depends on T. We should comment that the apparent rate constant of the OH addition to benzene also depends on the reaction time. Experimental kinetic measurements were typically made on the millisecond time scale. Our calculations show that low-P rate constants are essentially independent of t on the experimental time scale (t < 50 ms) at RT but not at 350 K. The time dependence of the apparent rate constant at higher T is caused by the decomposition of the C_6H_6-OH adduct back to reactants, which gains in importance soon after a large enough concentration of the adduct is accumulated. In our model, the apparent rate constant eventually drops to the rate of C_6H_5OH + H production because no other consumption channels are included. However, in the experiment of Goumri et al.,[18] the excess of radical scavengers was used to suppress the C_6H_6OH accumulation. As a result, the apparent rate constant may not be affected by the reverse decomposition even at very long reaction times. In our calculation of the P effect at 350 K, we used an artificially shortened reaction time of 1 ms instead of the experimental 10−50 ms. This allowed

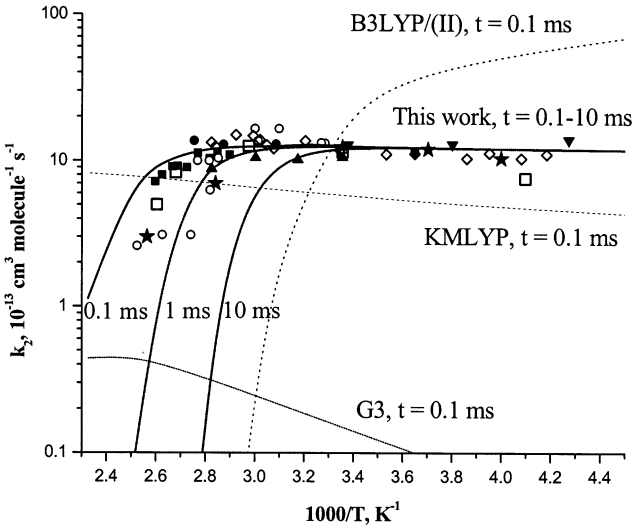

Figure 11. T and t dependencies of the apparent rate constant for the OH addition to benzene at $P = 133$ mbar (Ar). Experimental data: Tully et al.[7] (★), Lorenz and Zellner[8] (□), Witte et al.[10] (◇), Lin et al.[11] (■), Knispel et al.[17] (▲), Wallington et al.[9] (▼), Semadeni et al.[12] (●), Perry et al.[6] (○). Theoretical curves: G3 ($E_2 = 2.8$ kcal/mol, $E_{-2} = 19.1$ kcal/mol); B3LYP/(II) ($E_2 = -0.8$ kcal/mol, $E_{-2} = 12.4$ kcal/mol); KMLYP ($E_2 = 0.6$ kcal/mol, $E_{-2} = 22.2$ kcal/mol); this work ($E_2 = 0.1$ kcal/mol, $E_{-2} = 17.1$ kcal/mol).

us to account for the observed P effect without modifying our model to include all secondary reactions explicitly.

The effect of reaction time is shown in more detail in Figure 11, where we also illustrate the T dependence of the apparent rate constant k_2. We can see that it is essentially independent of t at $T < 300$ K on the millisecond time scale and that it has a very weak T dependence: $k^{\infty}_2(200-300\ \text{K}) = (1.2-1.4) \times 10^{-12}$ cm^3 molecule^{-1} s^{-1}. All low-T measurements were performed near HPL, and their results agree well with our calculated values of k^{∞}_2. The experimental kinetic data is much more scattered at higher T, where the time and T dependencies of k_2 become very strong. Since all reported rate constants are much higher than the computed values at 10 ms, the secondary reactions of the C_6H_6OH radical must be responsible for its consumption. The presence of radical scavengers, the total radical concentration, and other experimental conditions may affect the rates of these secondary reactions and the apparent total rate. The variation of these factors in different experiments is probably responsible for the large scatter of the experimental kinetic data at $T > 300$ K.

Conclusions

The mechanism of the addition and abstraction modes of the OH radical attack on benzene has been investigated by various ab initio and DFT methods. Different approaches to geometry optimization and energetics have been examined. The comparison with available experimental data indicates that the B3LYP density functional affords more accurate molecular parameters for the present system than the MP2, KMLYP, and MPW1K methods.

The OH-addition channel involves a $[C_6H_6\cdots HO]$ prereaction complex. Its molecular structure is found to be very flexible with respect to OH migration along and across the aromatic ring and OH rotation from a vertical to nearly horizontal orientation above the C_6H_6 plane. The lowest-energy conformation remains questionable, but the stabilization energy of this intermolecular complex is no less than 2.6 kcal/mol on the basis of the BSSE and ZPE-corrected G3 dissociation energy of the $[C_6H_6\cdots HO]$-C_{6v} conformation.

Both frontier MO analysis and the shape of the OH-addition profile support the dominant role of electrostatic and dispersion interactions rather than short-range MO interactions in the benzene−OH intermolecular attraction in the interval from $C_6H_6 + OH$ to the $[C_6H_6\cdots HO]$ prereaction complex. The molecular structures of the C_6H_6 and OH fragments remain virtually the same in this interval as in the pure reactants. At shorter intermolecular separations, the frontier MO interactions play an important role in the mechanism of the OH addition to benzene. The overlap of the β-HOMO of benzene with the β-LUMO of OH is the most important among them, and it determines the reactivity of an aromatic substrate toward transformation from the $[C_6H_6\cdots HO]$ van der Waals complex to the *ipso*-C_6H_6OH radical.

Reaction barriers had to be adjusted to better reproduce the most-reliable experimental kinetic data. Within its uncertainty, the following estimates of the 0 K reaction barriers have been derived: 3.5 kcal/mol $\le E_1 \le$ 5.0 kcal/mol (abstraction channel) and $E_2 = 0.1 \pm 0.1$ kcal/mol (addition channel). A relatively large uncertainty in the H-abstraction barrier is due to the questionable interpretation of the high-T kinetic data ($T > 390$ K) in terms of the abstraction mechanism alone, as typically reported in all high-T measurements of the $C_6H_6 + OH$ reaction. Inconsistencies in the reported k_1 rate constants and kinetic isotope effects have been identified, which prevent us from giving a more precise estimate of E_1.

From first principles, the G3 theoretical scheme predicts the most-reliable energetic parameters but tends to overestimate the reaction barriers. Nevertheless, the theoretical predictions show a considerable improvement compared to the previous generation of G2M theory. Within the DFT framework alone, the B3LYP, KMLYP, and MPW1K density functionals may be used for survey calculations to identify the most-important reaction channels. These relatively fast calculations may provide the upper (MPW1K) and lower (B3LYP) bounds for questionable reaction barriers, as appears from a limited comparison for reactions relevant to this study. The KMLYP method reproduces the barriers of reactions 1 and 2 remarkably well. However, none of these functionals can deliver consistently good performance for different chemical processes.

On the basis of deduced (i.e., reaction barriers, collisional energy transfer parameters) and predicted (i.e., molecular parameters) theoretical parameters, the final kinetic model for the OH-addition channel that includes barrierless association, two-well isomerization, collisional stabilization and excitation, and unimolecular decomposition of the chemically activated intermediates has been constructed. Except for the P-dependence studies of Davis et al.[34] and Baulch et al.,[35] available kinetic data for the OH-addition channel can be accurately accounted for with our calculated (P, T)-dependent effective rate constants. H-for-OH exchange reaction 3 is predicted to be negligible compared to H-abstraction channel 1 over the wide T range (200−2500 K). Upon its extension to include secondary reactions of the C_6H_6OH radical, the present model can be utilized for larger-scale gas-phase systems containing C_6H_6 and OH.

Acknowledgment. We are grateful for the support of this work from the Department of Energy, Office of Basic Energy Sciences, Division of Chemical Sciences through contract DE-FGO2-97ER14784. Our special thanks go to the authors of the ChemRate program, in particular to Vladimir Mokrushin and Vadim Knyazev, for enriching discussions and live updates of

this software package. Also, we are thankful to the Cherry L. Emerson Center of Emory University for the use of its resources, which are in part supported by a National Science Foundation grant (CHE-0079627) and an IBM Shared University Research Award.

Appendix

The rate of the H-for-OH desubstitution in the reaction of phenol with H has been measured by He, Mallard, and Tsang[13] and by Manion and Louw.[14,15] The absolute values of the $k_{(-3)}$ rate constant derived in these studies are in good agreement. However, the T range where the experiments were conducted was relatively narrow (922−1180 K), and activation parameters derived from the Arrhenius fits are markedly different. The experimental and theoretical values of $k_{(-3)}$ are plotted in Figure A1. The theoretical predictions were derived by the same approaches as discussed previously for reaction 1. As follows from Figure A1, all experimental data can be accurately accounted for by theory with the energy barrier of $E_{(-3)}^0 = 8.0 \pm 0.5$ kcal/mol. The G2M and G3 methods overestimate the fitted barrier by 3.8 and 1.9 kcal/mol, respectively. The rate constants calculated from the MPW1K/(I) energetic and molecular parameters agree with the experimental values surprisingly well, whereas the B3LYP/(II) and KMLYP/(I) estimates are somewhat too high. The following expression gives the best theoretical prediction of the H-for-OH desubstitution rate constant based on the adjusted barrier of 8.0 kcal/mol: $k_{(-3)} = 8.9 \times 10^{-18} T^{2.0} \exp(-2753 \pm 250/T)$ cm^3 molecule^{-1} s^{-1}, where $T = 200-2500$ K. Interestingly, the substituent effects on the enthalpies and the barriers of H addition to various aromatic substrates show excellent correlation for a series of monosubstituted benzenes. An increase in the enthalpies of the H + C_6H_5X addition reactions from 17.0 kcal/mol (X = OH) to 20.1 kcal/mol (X = CH_3)[47] to 21.3 kcal/mol (X = H)[47] is paralleled by a decrease in the barriers from 8.0 kcal/mol (X = OH) to 6.0 kcal/mol (X = CH_3)[47] to 5.2 kcal/mol (X = H).[47] For any pair of substituents, the difference in the barriers for H addition at the ipso position is about $^2/_3$ of the difference in the enthalpies of the corresponding reactions.

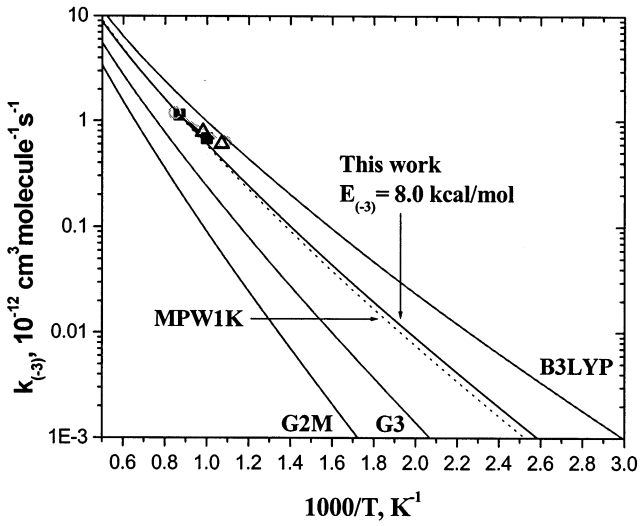

Figure A1. Arrhenius plot of the rate constant for the C_6H_5OH + H = C_6H_6 + OH reaction. Four theoretical curves are calculated by conventional TST with Eckart tunneling corrections based on B3LYP/(II), MPW1K, G2M, and G3 molecular and energetic parameters. The recommended rate constant is based on the adjusted reaction barrier of 8.0 kcal/mol. Experimental values are taken from He et al.[13] (■) and Manion and Louw (○ from ref 15, △ from ref 14).

With the expressions for K_3 and $k_{(-3)}$ in hand, we can estimate the k_3 rate constant as the product of K_3 and $k_{(-3)}$: $k_3 = 5.0 \times 10^{-24} T^{3.62} \exp(-2443 \pm 250/T)$. Assuming the validity of this estimate, we conclude that the importance of reaction 3 compared to abstraction channel 1 is negligibly small (less than 5%) at $T = 200-2500$ K.

Supporting Information Available: Molecular parameters for various species calculated by the MP2/(I), MPW1K/(I), and KMLYP/(I) methods (Tables S1 and S2). This material is available free of charge via the Internet at http://pubs.acs.org.

References and Notes

(1) Tsang, W. *Chem. Phys. Processes Combust.* **2001**, 15−24.
(2) Baulch, D. L.; Cobos, C. J.; Cox, R. A.; Esser, C.; Frank, P.; Just, Th.; Kerr, J. A.; Pilling, M. J.; Troe, J.; Walker, R. W.; Warnatz, J. *J. Phys. Chem. Ref. Data* **1992**, *21*, 411−429 and references therein.
(3) (a) Atkinson, R. *Chem. Rev.* **1986**, *86*, 69−201. (b) Atkinson, R. *J. Phys. Chem. Ref. Data* **1989**, Monograph 1, 204 and references therein.
(4) Fujii, N.; Asaba, T. *J. Fac. Eng., Univ. Tokyo, Ser. B* **1977**, *34*, 189−224.
(5) (a) Madronich, S.; Felder, W. *J. Phys. Chem.* **1985**, *89*, 3556. (b) Felder, W.; Madronich, S. *Combust. Sci. Technol.* **1986**, *50*, 135−150.
(6) Perry, R. A.; Atkinson, R.; Pitts, J. N., Jr. *J. Phys. Chem.* **1977**, *81*, 296.
(7) Tully, F. P.; Ravishankara, A. R.; Thompson, R. L.; Nicovich, J. M.; Shah, R. C.; Kreutter, N. M.; Wine, P. H. *J. Phys. Chem.* **1981**, *85*, 2262.
(8) Lorenz, K.; Zellner, R. *Ber. Bunsen-Ges. Phys. Chem.* **1983**, *87*, 629; see also ref 2.
(9) Wallington, T. J.; Neuman, D. M.; Kurylo, M. J. *Int. J. Chem. Kinet.* **1987**, *19*, 725.
(10) (a) Witte, F.; Urbanik, E.; Zetzsch, C. *J. Phys. Chem.* **1986**, *90*, 3251. (b) Witte, F.; Zetzsch, C. *Phys. Chem. Behav. Atmos. Pollut., Proc. Eur. Symp.,3rd* **1984**, 168. (c) Rinke, M.; Zetzsch, C. *Ber. Bunsen-Ges. Phys. Chem.* **1984**, *88*, 55. (d) Wahner, A.; Zetzsch, C. *J. Phys. Chem.* **1983**, *87*, 4945.
(11) Lin, S.-C.; Kuo, T.-C.; Lee, Y.-P. *J. Chem. Phys.* **1994**, *101*, 2098−2105.
(12) Semadeni, M.; Stocker, D. W.; Kerr, J. A. *Int. J. Chem. Kinet.* **1995**, *27*, 287−304.
(13) He, Y. Z.; Mallard, W. G.; Tsang, W. *J. Phys. Chem.* **1988**, *92*, 2196−2201.
(14) Manion, J. A.; Louw, R. *J. Phys. Chem.* **1990**, *94*, 4127−4134.
(15) Manion, J. A.; Louw, R. *J. Phys. Chem.* **1989**, *93*, 3563.
(16) Mulder, P.; Louw, R. *Int. J. Chem. Kinet.* **1988**, *20*, 577−592.
(17) Knispel, R.; Koch, R.; Siese, M.; Zetzsch, C. *Ber. Bunsen-Ges. Phys. Chem.* **1990**, *94*, 1375−1379.
(18) Goumri, A.; Pauwels, J. F.; Devolder, P. *Can. J. Chem.* **1991**, *69*, 1057−1064.
(19) Lobanov, V. V.; Vysotskaya, N. A.; Rabovskaya, E. A.; Bogillo, V. I. *Teor. Eksp. Khim.* **1986**, *22*, 20.
(20) Lay, T. H.; Bozzelli, J. W.; Seinfeld, J. H. *J. Phys. Chem.* **1996**, *100*, 6543−6554.
(21) Cheney, B. V. *J. Mol. Struct.: THEOCHEM* **1996**, *364*, 219−237.
(22) Berho, F.; Rayez, M.-Th.; Lesclaux, R. *J. Phys. Chem. A* **1999**, *103*, 5501−5509.
(23) Barckholtz, C.; Barckholtz, T. A.; Hadad, C. *J. Phys. Chem. A* **2001**, *105*, 140−152.
(24) Ghigo, G.; Tonachini, G. *J. Am. Chem. Soc.* **1998**, *120*, 6753−6757.
(25) Ghigo, G.; Tonachini, G. *J. Am. Chem. Soc.* **1999**, *121*, 8366−8372.
(26) Motta, F.; Ghigo, G.; Tonachini, G. *J. Phys. Chem. A* **2002**, *106*, 4411−4422.
(27) Bjergbakke, E.; Sillesen, A.; Pagsberg, P. *J. Phys. Chem.* **1996**, *100*, 5729−5736.
(28) Berndt, T.; Boge, O.; Herrmann, H. *Chem. Phys. Lett.* **1999**, *314*, 435−442.
(29) Atkinson, R.; Aschmann, S. M.; Arey, J.; Carter, W. P. L. *Int. J. Chem. Kinet.* **1989**, *21*, 801.
(30) Bohn, B.; Zetzsch, C. *Phys. Chem. Chem. Phys.* **1999**, *1*, 5097−5107.
(31) Klopffer, V. W.; Frank, R.; Kohl, E.-G.; Haag, F. *Chem. -Ztg.* **1986**, *110*, 57−62.
(32) Edney, E. O.; Kleindienst, T. E.; Corse, E. W. *Int. J. Chem. Kinet.* **1986**, *18*, 1355.
(33) Ohta, T.; Ohyama, T. *Bull. Chem. Soc. Jpn.* **1985**, *58*, 3029.

(34) Davis, D. D.; Bollinger, W.; Fischer, S. *J. Phys. Chem*. **1975**, *79*, 293.
(35) Baulch, D. L.; Campbell, I. M.; Saunders, S. M. *J. Chem. Soc., Faraday Trans. 2* **1988**, *84*, 377.
(36) Hansen, D. A.; Atkinson, R.; Pitts, J. N., Jr. *J. Phys. Chem*. **1975**, *79*, 1763.
(37) Cox, R. A.; Derwent, R. G.; Williams, M. R. *Environ. Sci. Technol*. **1980**, *14*, 57.
(38) (a) Lin, C. Y.; Lin, M. C. *Chem. Phys. Processes Combust*. **1984**, 86/1−86/4. (b) Hsu, D. S. Y.; Lin, C. Y.; Lin, M. C. *Proc. Int. Symp. Combust*. **1984**, *20*, 623−30.
(39) (a) Becke, A. D. *J. Chem. Phys*. **1993**, *98*, 5648. (b) Becke, A. D. *Phys. Rev. A* **1988**, *38*, 3098. (c) Lee, C.; Yang, W.; Parr, R. G. *Phys. Rev. B* **1988**, *37*, 785. (d) Stephens, P. J.; Devlin, F. J.; Chabalowski, C. F.; Frisch, M. J. *J. Phys. Chem*. **1994**, *98*, 11623.
(40) Lynch, B. J.; Fast, P. L.; Harris, M.; Truhlar, D. G. *J. Phys. Chem. A* **2000**, *104*, 4811−4815.
(41) Kang, J. K.; Musgrave, Ch. B. *J. Chem. Phys.* **2001**, *115*, 11040−11050.
(42) Gonzalez, C.; Schlegel, H. B. *J. Chem. Phys.* **1989**, *90*, 2154−2161. Gonzalez, C.; Schlegel, H. B. *J. Phys. Chem*. **1990**, *94*, 5523−5527.
(43) Pople, J. A.; Head-Gordon, M.; Raghavachari, K. *J. Chem. Phys*. **1987**, *87*, 5768.
(44) Mebel, A. M.; Morokuma, K.; Lin, M. C. *J. Chem. Phys*. **1995**, *103*, 7414.
(45) Curtiss, L. A.; Raghavachari, K.; Redfern, P. C.; Rassolov, V.; Pople, J. A. *J. Chem. Phys*. **1998**, *109*, 7764.
(46) Bacskay, G. B. *Chem. Phys.* **1981**, *61*, 385−404.
(47) Tokmakov, I. V.; Lin, M. C. *Int. J. Chem. Kinet*. **2001**, *33*, 633−653.
(48) Curtiss, L. A.; Raghavachari, K.; Trucks, G. W.; Pople, J. A. *J. Chem. Phys*. **1991**, *94*, 7221.
(49) Baboul, A. G.; Curtiss, L. A.; Redfern, P. C.; Raghavachari, K. *J. Chem. Phys*. **1999**, *110*, 7650.
(50) Curtiss, L. A.; Redfern, P. C.; Raghavachari, K.; Pople, J. A. *J. Chem. Phys*. **2001**, *114*, 108.
(51) Tokmakov, I. V.; Park, J.; Gheyas, S.; Lin, M. C. *J. Phys. Chem. A* **1999**, *103*, 3636−3645.
(52) Frisch, M. J.; Trucks, G. W.; Schlegel, H. B.; Scuseria, G. E.; Robb, M. A.; Cheeseman, J. R.; Zakrzewski, V. G.; Montgomery, J. A., Jr.; Stratmann, R. E.; Burant, J. C.; Dapprich, S.; Millam, J. M.; Daniels, A. D.; Kudin, K. N.; Strain, M. C.; Farkas, O.; Tomasi, J.; Barone, V.; Cossi, M.; Cammi, R.; Mennucci, B.; Pomelli, C.; Adamo, C.; Clifford, S.; Ochterski, J.; Petersson, G. A.; Ayala, P. Y.; Cui, Q.; Morokuma, K.; Malick, D. K.; Rabuck, A. D.; Raghavachari, K.; Foresman, J. B.; Cioslowski, J.; Ortiz, J. V.; Stefanov, B. B.; Liu, G.; Liashenko, A.; Piskorz, P.; Komaromi, I.; Gomperts, R.; Martin, R. L.; Fox, D. J.; Keith, T.; Al-Laham, M. A.; Peng, C. Y.; Nanayakkara, A.; Gonzalez, C.; Challacombe, M.; Gill, P. M. W.; Johnson, B. G.; Chen, W.; Wong, M. W.; Andres, J. L.; Head-Gordon, M.; Replogle, E. S.; Pople, J. A. *Gaussian 98*, revision A.7; Gaussian, Inc.: Pittsburgh, PA, 1998.
(53) Mokrushin, V.; Bedanov, V.; Tsang, W.; Zachariah, M.; Knyazev, V. *ChemRate*, version 1.19; NIST: Gaithersburg, MD, 2002.
(54) Forst, W. *Theory of Unimolecular Reactions*; Academic Press: New York, 1973.
(55) Gilbert, R. G.; Smith, S. C. *Theory of Unimolecular and Recombination Reactions*; Blackwell Scientific Publications: Oxford, U.K., 1990.
(56) Robinson, P. J.; Holbrook, K. A. *Unimolecular Reactions*; Wiley: New York, 1972.
(57) Astholz, D. C.; Troe, J.; Wieters, W. *J. Chem. Phys*. **1979**, *70*, 5107.
(58) Rabinovitch, B. S.; Tardy, D. C. *J. Chem. Phys*. **1966**, *45*, 3720.
(59) Reid, R. C.; Prausnitz, J. M.; Sherwood, T. K. *The Properties of Gases and Liquids*, 3rd ed.; McGraw-Hill: New York, 1977.
(60) Wilkinson, J. H.; Reinsch, C. *Linear Algebra*; Springer: New York, 1971.
(61) (a) Tsang, W.; Bedanov, V.; Zachariah, M. R. *J. Phys. Chem*. **1996**, *100*, 4011. (b) Bedanov, V. M.; Tsang, W.; Zachariah, M. R. *J. Phys. Chem*. **1995**, *99*, 11452. (c) Knyazev, V. D.; Tsang, W. *J. Phys. Chem. A* **1999**, *103*, 3944. (d) Knyazev, V. D.; Tsang, W. *J. Phys. Chem. A* **2000**, *104*, 10747.
(62) Chase, M. W., Jr. NIST-JANAF Thermochemical Tables, 4th ed.; In *J. Phys. Chem. Ref. Data;* Monograph No. 9; American Chemical Society: Washington, DC, 1998.
(63) (a) Cabana, A.; Bachand, J.; Giguere, J. *Can. J. Phys.* **1974**, *52*, 1949. (b) Tamagawa, K.; Iijima, T.; Kimura, M. *J. Mol. Struct.* **1976**, *30*, 243.
(64) (a) Portalone, G.; Schultz, G.; Domenicano, A.; Hargittai, I. *Chem. Phys. Lett*. **1992**, *197*, 482−488. (b) Larsen, N. W. *J. Mol. Struct*. **1979**, *51*, 175.
(65) Snels, M.; Hellenstein, H.; Quack. M. *Chem. Phys*. **1997**, *225*, 107 and references therein.
(66) Frenkel, M.; Marsh, K. N.; Wilhoit, R. C.; Kabo, G. J.; Roganov, G. N. *Thermodynamics of Organic Compounds in the Gas Phase*; Thermodynamics Research Center: College Station, TX, 1994.
(67) Lapinski, A.; Spanget-Larsen, J.; Langgard, M.; Waluk, J.; Radziszewski, J. G. *J. Phys. Chem. A* **2001**, *105*, 10520−10524.
(68) Friderichsen, A. V.; Radziszewski, J. G.; Juliusz, G.; Nimlos, M. R.; Winter, P. R.; Dayton, D. C.; David, D. E.; Ellison, G. B. *J. Am. Chem. Soc.* **2001**, *123*, 1977−1988.
(69) Lapinski, A.; Spanget-Larsen, J.; Langgard, M.; Waluk, J.; Radziszewski, J. G. *J. Phys. Chem. A* **2001**, *105*, 10520−10524.
(70) Radziszewski, J. G.; Nimlos, M. R.; Winter, P. R.; Ellison, G. B. *J. Am. Chem. Soc.* **1996**, *118*, 7400−7401.
(71) Scott, A. P.; Radom, L. *J. Phys. Chem*. **1996**, *100*, 16502.
(72) Pitzer, K. S.; Gwinn, W. D. *J. Chem. Phys*. **1942**, *10*, 428.
(73) Boys, S. F.; Bernardi, F. *Mol. Phys.* **1970**, *19*, 553.
(74) Pedley, J. B. *Thermodynamic Data and Stuctures of Organic Compounds*; Thermodynamics Research Center: College Station, TX, 1994; Vol. 1.
(75) Ruscic, B. Private communication. A slightly different value of $\Delta_f H°298(OH) = 8.89 \pm 0.09$ kcal/mol was reported in the initial letter; Ruscic, B.; Feller, D.; Dixon, D. A.; Peterson, K. A.; Harding, L. B.; Asher, R. L.; Wagner, A. F. *J. Phys. Chem. A* **2001**, *105*, 1−4.
(76) Ruscic, B.; Litorja, M.; Asher, R. L. *J. Phys. Chem. A* **1999**, *103*, 8625. Ruscic, B.; Litorja, M.; Asher, R. L. *J. Phys. Chem. A* **2000**, *104*, 8600.
(77) Davico, G. E.; Bierbaum, V. M.; DePuy, C. H.; Ellison, G. B.; Squires, R. R. *J. Am. Chem. Soc*. **1995**, *117*, 2590−2599.
(78) (a) Furuyama, S.; Golden, D. M.; Benson, S. W. *J. Chem. Thermodyn*. **1969**, *1*, 363. (b) Lacher, J. R.; Walden, C. H.; Lea, K. R.; Park, J. D. *J. Am. Chem. Soc*. **1950**, *72*, 331−333.
(79) Sosa, C.; Schlegel, H. B. *J. Am. Chem. Soc*. **1987**, *109*, 4193.
(80) Alvarez-Idaboy, J. R.; Mora-Diez, N.; Vivier-Bunge, A. *J. Am. Chem. Soc*. **2000**, *122*, 3715−3720.
(81) Sekusak, S.; Liedl, K. R.; Sabljic, A. *J. Phys. Chem. A* **1998**, *102*, 1583−1594.
(82) Piqueras, M. C.; Crespo, R.; Nebot-Gil, I.; Tomas, F. *J. Mol. Struct.: THEOCHEM* **2001**, *537*, 199−212.
(83) Eckart, C. *Phys. Rev*. **1930**, *35*, 1303.
(84) Mebel, A. M.; Lin, M. C.; Yu, T.; Morokuma, K. *J. Phys. Chem. A* **1997**, *101*, 3189−3196.
(85) (a) Robertson, S. H.; Wagner, A. F.; Wardlaw, D. M. *Faraday Discuss*. **1995**, *102*, 65−83. (b) Robertson, S. H.; Wagner, A. F.; Wardlaw, D. M. *J. Chem. Phys*. **1995**, *103*, 2917−2928.

(86) Under these conditions, the prereaction complex is very unstable, but the C_6H_6OH radical is stable. Then scheme II can be simplified as follows:

$$C_6H_6 + OH(+M) \underset{-k_{vdW}}{\overset{k_{vdW}}{\rightleftharpoons}} [C_6H_6\cdots HO](+M) \xrightarrow{k_{2'}} C_6H_6OH(+M)$$

A fast equilibrium exists between the reactants and their loosely bonded complex ($k_{-vdW} \gg k_{2'}$). The steady-state analysis for this kind of system[80] leads to the apparent rate constant that is essentially independent of the properties of TS-vdW and $[C_6H_6\cdots OH]$: $k_2 \approx (\kappa/\beta h)\,(Q_{TS2}/Q_R)\exp(-\beta E_2)$, where κ is the tunneling factor and Q_{TS2} and Q_R are partition functions of TS2 and the reactants.